Journal of the Mechanics and Physics of Solids ▮ (▮▮▮▮) ▮▮▮–▮▮▮

Contents lists available at ScienceDirect

Journal of the Mechanics and Physics of Solids

journal homepage: www.elsevier.com/locate/jmps

Cavitation in elastomeric solids: II—Onset-of-cavitation surfaces for Neo-Hookean materials

Oscar Lopez-Pamies [a,*], Toshio Nakamura [a], Martín I. Idiart [b,c]

[a] Department of Mechanical Engineering, State University of New York, Stony Brook, NY 11794-2300, USA
[b] Departamento de Aeronáutica, Facultad de Ingeniería, Universidad Nacional de La Plata, Calles 1 y 47, La Plata B1900TAG, Argentina
[c] Consejo Nacional de Investigaciones Científicas y Técnicas (CONICET), Avda. Rivadavia 1917, Cdad. de Buenos Aires C1033AAJ, Argentina

ARTICLE INFO

Article history:
Received 3 November 2010
Received in revised form
15 April 2011
Accepted 16 April 2011

Keywords:
Finite strain
Microstructures
Instabilities
Bifurcation
Failure surfaces

ABSTRACT

In Part I of this work we derived a fairly general theory of cavitation in elastomeric solids based on the sudden growth of pre-existing defects. In this article, the theory is used to determine onset-of-cavitation surfaces for Neo-Hookean solids where the defects are isotropically distributed and vacuous. These surfaces correspond to the set of all critical Cauchy stress states at which cavitation ensues; general three-dimensional loadings are considered. Their computation requires the numerical solution of a nonlinear first-order partial differential equation in two variables. The theoretical results indicate that cavitation occurs only for stress states where the three principal Cauchy stresses are tensile, and that the required hydrostatic tensile component increases with increasing shear components. These results are confronted to finite-element simulations for the growth of a small spherical cavity in a Neo-Hookean block under multi-axial loading. Good agreement is found for a wide range of loading conditions. Comparisons with earlier results available in the literature are also provided and discussed. We conclude this work by devising a *closed-form* approximation to the theoretical surface, which is of remarkable accuracy and mathematical simplicity.

1. Introduction

In the preceding paper Lopez-Pamies et al. (in press), henceforth referred to as Part I, we proposed a new strategy to study cavitation in elastomeric solids. The basic idea was to first cast this phenomenon as the homogenization problem of nonlinear elastic materials containing random distributions of *defects*, which were modeled as disconnected nonlinear elastic cavities of zero volume, but of arbitrary shape otherwise. By means of a novel iterated homogenization technique, we then constructed solutions for a specific but fairly general class of distributions and shapes of defects. These included solutions for the change in volume fraction of the underlying defects as a function of the applied loading conditions, from which the onset of cavitation — corresponding to the event when the initially infinitesimal volume fraction of defects suddenly grows into finite values — could be determined. The distinctive features of the theory are that it: (i) allows to consider 3D general loading conditions with arbitrary triaxiality, (ii) is applicable to large (including compressible and anisotropic) classes of nonlinear elastic solids, (iii) incorporates direct information on the initial shape, spatial distribution, and mechanical properties of the underlying defects at which cavitation can initiate, and, in spite of accounting for this

* Corresponding author. Tel.: +1 631 632 8249; fax: +1 631 632 8544.
E-mail addresses: oscar.lopez-pamies@sunysb.edu (O. Lopez-Pamies), toshio.nakamura@sunysb.edu (T. Nakamura), martin.idiart@ing.unlp.edu.ar (M.I. Idiart).

0022-5096/$ - see front matter © 2011 Elsevier Ltd. All rights reserved.
doi:10.1016/j.jmps.2011.04.016

refined information, (iv) is computationally tractable since the relevant analysis reduces to the study of two Hamilton–Jacobi equations in which the initial volume fraction of defects plays the role of "time" and the applied load plays the role of "space".

The objective of this paper is to make use of the theory developed in Part I for the first time. Motivated by an application of practical interest that at the same time can lead to results that are as explicit as possible, the problem that we consider here is the construction of an onset-of-cavitation criterion for Neo-Hookean materials, in which the underlying defects are *isotropically distributed* and *vacuous*, under general 3D loading conditions. In this regard, it is appropriate to remark that the Neo-Hookean material model describes reasonably well the response of vulcanized natural rubber (Treloar, 1944), as well as that of other commercially utilized elastomers (see, e.g., Lopez-Pamies, 2010), over a wide range of deformations.[1] Moreover, the distribution of defects is expected to indeed be isotropic within elastomers prepared by most typical processes of synthesis/fabrication. On the other hand, the assumption that the defects are vacuous is adopted here mainly for computational simplicity, but also partly for lack of a better experimentally based constitutive prescription. The emphasis of the selected application aims then at shedding light on the effect of load triaxiality on the onset of cavitation in standard rubber. In this connection, it is important to recall that the majority of cavitation analyses available in the literature have restricted attention to pure hydrostatic loading conditions (Horgan and Polignone, 1995; Fond, 2001). Yet, the occurrence of cavitation is expected to depend sensitively on the triaxiality of the applied loading, and not just on the hydrostatic component (Gent and Tompkins, 1969; Chang et al., 1993; Bayraktar et al., 2008). The results to be generated in this paper seek to quantify this dependence.

In addition to the analytical results derived from the theory of Part I, in this work we also generate numerical finite-element (FE) results for the onset of cavitation in Neo-Hookean materials under general loading conditions. More specifically, our strategy is to generate full 3D solutions for the large-deformation response of a Neo-Hookean block that contains an initially small, vacuous, spherical cavity located at its center. The critical loads at which cavitation occurs are then identified as the affine loads externally applied to the block at which the initially small cavity suddenly grows to a much larger size. While this numerical approach seems simple enough, its presentation in the literature is not known to the authors.

In Section 2, for convenience and clarity, we recall the cavitation criterion developed in Part I for the case when the defects at which cavitation can initiate are isotropically distributed and vacuous. Section 3 deals with the further specialization of this criterion to Neo-Hookean materials and presents the main result of the paper: *inside a Neo-Hookean material, cavitation occurs at a material point P whenever along a given loading path the principal Cauchy stresses* t_i $(i=1,2,3)$ *at that point first satisfy the condition*

$$8t_1t_2t_3-12\mu(t_1t_2+t_1t_3+t_2t_3)\Psi+18\mu^2(t_1+t_2+t_3)\Psi^2-27\mu^3\Psi^3-8\mu^3=0 \quad \text{with } t_i>0, \tag{1}$$

where μ denotes the shear modulus of the material in its undeformed state, and $\Psi=\Psi(t_2-t_1,t_3-t_1)$ that satisfies $0<\Psi\leq 1$ and is solution of a first-order nonlinear partial differential equation (pde). Section 4 describes the FE calculations. The analytical and numerical onset-of-cavitation surfaces constructed in Sections 3 and 4 are plotted, discussed, and compared with earlier results in Section 5. Finally, we show in Section 6 that the *closed-form* criterion

$$8t_1t_2t_3-12\mu(t_1t_2+t_1t_3+t_2t_3)+18\mu^2(t_1+t_2+t_3)-35\mu^3=0 \quad \text{with } t_i>0 \tag{2}$$

is a remarkably accurate approximation of the exact criterion (1), which in fact can be utilized in lieu of (1) for all practical purposes.

2. Cavitation criterion: the case of isotropically distributed vacuous defects

In Part I, guided by experimental evidence (Gent, 1991), we considered the phenomenon of cavitation in elastomeric solids as the sudden growth of defects present in a nonlinear elastic material in response to sufficiently large applied external loads. In particular, we considered that the pre-existing defects at which cavitation can initiate are nonlinear elastic cavities of zero volume, but of arbitrary shape otherwise, that are randomly distributed throughout the solid. This point of view led to formulating the problem of cavitation as the homogenization problem of nonlinear elastic materials containing zero-volume cavities, which in turn led to the construction of a fairly general — yet computationally tractable — cavitation criterion. For the case of interest here, when the underlying defects are *isotropically distributed* and *vacuous*, the criterion can be written as follows:

> The onset of cavitation in a nonlinear elastic material with stored-energy function $W(\mathbf{F})$ occurs at critical values $\mathbf{F}_{cr}$ of the deformation gradient tensor $\mathbf{F}$ such that
>
> $$\mathbf{F}_{cr}\in\partial\mathcal{Z}[f_\star(\mathbf{F})] \quad \text{and} \quad 0<\|\mathbf{S}_\star(\mathbf{F}_{cr})\|<+\infty, \tag{3}$$

[1] The Neo-Hookean model has the further merit that it is derivable from statistical mechanics (Treloar, 1943).

Please cite this article as: Lopez-Pamies, O., et al., Cavitation in elastomeric solids: II—Onset-of-cavitation surfaces for Neo-Hookean materials. J. Mech. Phys. Solids (2011), doi:10.1016/j.jmps.2011.04.016

where $\partial\mathcal{Z}[f_\star(\mathbf{F})]$ denotes the boundary of the zero set of $f_\star(\mathbf{F})$ and $\|\mathbf{S}_\star(\mathbf{F}_{cr})\|$ indicates the Euclidean norm of $\mathbf{S}_\star(\mathbf{F}_{cr})$ with

$$f_\star(\mathbf{F}) \doteq \lim_{f_0\to 0+} f(\mathbf{F},f_0) \quad \text{and} \quad \mathbf{S}_\star(\mathbf{F}) \doteq \lim_{f_0\to 0+} \frac{\partial E}{\partial \mathbf{F}}(\mathbf{F},f_0). \tag{4}$$

Here, the scalar functions $E(\mathbf{F}, f_0)$ and $f(\mathbf{F}, f_0)$ are defined by the initial-value problems

$$f_0\frac{\partial E}{\partial f_0} - E - \max_{\boldsymbol{\omega}(\xi)} \int_{|\xi|=1} \frac{1}{4\pi}\left[\boldsymbol{\omega}\cdot\frac{\partial E}{\partial \mathbf{F}}\xi - W(\mathbf{F}+\boldsymbol{\omega}\otimes\xi)\right] \mathrm{d}\xi = 0, \quad E(\mathbf{F},1)=0 \tag{5}$$

and

$$f_0\frac{\partial f}{\partial f_0} - f - \frac{f}{4\pi}\int_{|\xi|=1} \boldsymbol{\omega}\cdot\mathbf{F}^{-T}\xi \,\mathrm{d}\xi - \frac{1}{4\pi}\int_{|\xi|=1} \boldsymbol{\omega}\cdot\frac{\partial f}{\partial \mathbf{F}}\xi \,\mathrm{d}\xi = 0, \quad f(\mathbf{F},1)=1, \tag{6}$$

where $\boldsymbol{\omega}$ in (6) denotes the maximizing vector $\boldsymbol{\omega}$ in (5). The corresponding first Piola–Kirchhoff and Cauchy critical stresses at cavitation are given respectively by

$$\mathbf{S}_{cr} = \mathbf{S}_\star(\mathbf{F}_{cr}) \quad \text{and} \quad \mathbf{T}_{cr} = \frac{1}{\det \mathbf{F}_{cr}}\mathbf{S}_{cr}\mathbf{F}_{cr}^T. \tag{7}$$

The function E defined by (5) represents physically the total elastic energy (per unit undeformed volume) characterizing the homogenized constitutive response of a nonlinear elastic material with stored-energy function W containing a certain isotropic distribution of disconnected vacuous cavities of initial volume fraction f_0. The function f defined by (6), on the other hand, characterizes the evolution of the volume fraction of the cavities along finite-deformation loading paths. The asymptotic behavior (4) of these functions (in the limit as $f_0\to 0+$ when the underlying cavities become *point defects*) are the quantities that serve to identify the critical deformations (3) and critical stresses (7) at which cavitation occurs. For a detailed description of the derivation and of the various quantities involved in the above criterion, we refer to Section 4 of Part I.

From a computational point of view, it is important to remark that the first-order pdes $(5)_1$ and $(6)_1$ correspond to Hamilton–Jacobi equations, where the initial volume fraction of cavities f_0 and the deformation gradient $\mathbf{F}$ play the roles of "time" and "space" variables, respectively (Polyanin et al., 2002). Because of the ubiquitousness of Hamilton–Jacobi equations in physics, a large number of techniques for solving this class of pdes have been developed over the years (see, e.g., Benton, 1977; Polyanin et al., 2002). Hence, in spite of its generality, the criterion (3)–(7) is computationally tractable and thus expected to be useful for generating explicit results.

2.1. Incompressible isotropic solids

When the nonlinear elastic material of interest satisfies internal constraints and/or exhibits some type of material symmetry, the cavitation criterion (3)–(7) can be simplified significantly. Because of its physical relevance for actual elastomers, and for later use in the application to Neo-Hookean materials, we spell out next the specialization of the above criterion to *incompressible isotropic* solids with stored-energy function[2]

$$W(\mathbf{F}) = \begin{cases} \phi(\lambda_1,\lambda_2,\lambda_3) & \text{if } \det\mathbf{F} = \lambda_1\lambda_2\lambda_3 = 1, \\ +\infty & \text{otherwise,} \end{cases} \tag{8}$$

where ϕ is a symmetric function of the eigenvalues (or principal stretches) $\lambda_1,\lambda_2,\lambda_3$ of $(\mathbf{F}^T\mathbf{F})^{1/2}$.

As discussed in Section 4.1 of Part I, the kinematical constraint of incompressibility in (8) implies that the maximizing vector $\boldsymbol{\omega}$ in (5) must satisfy the constraint

$$\boldsymbol{\omega}\cdot\mathbf{F}^{-T}\xi = \frac{1-\det\mathbf{F}}{\det\mathbf{F}}, \tag{9}$$

and that the current volume fraction of cavities f defined by (6) simplifies to the explicit form

$$f(\mathbf{F},f_0) = \frac{\det\mathbf{F}-1}{\det\mathbf{F}} + \frac{f_0}{\det\mathbf{F}}. \tag{10}$$

Moreover, as discussed in Section 4.2 of Part I, the overall[3] isotropy of this problem implies that the corresponding total elastic energy E defined by (5) only depends on $\mathbf{F}$ through the principal stretches, so that — with a slight abuse of notation — we can write

$$E(\mathbf{F},f_0) = E(\lambda_1,\lambda_2,\lambda_3,f_0). \tag{11}$$

[2] Subsequently, the unbounded branch of the stored-energy function for non-isochoric deformations will be omitted for notational simplicity.

[3] The material behavior (8) is *constitutively isotropic* and the distribution of the vacuous cavities is *geometrically isotropic*.

Please cite this article as: Lopez-Pamies, O., et al., Cavitation in elastomeric solids: II—Onset-of-cavitation surfaces for Neo-Hookean materials. J. Mech. Phys. Solids (2011), doi:10.1016/j.jmps.2011.04.016

A second implication of overall isotropy is that it suffices to restrict attention, without loss of generality, to pure stretch deformation gradients of the diagonal form

$$F_{ij} = \mathrm{diag}(\lambda_1,\lambda_2,\lambda_3). \tag{12}$$

Making direct use of relations (8)–(12) in the general expressions (3)–(7) allows to state the cavitation criterion in the following more explicit form:

The onset of cavitation in an incompressible isotropic nonlinear elastic material with stored-energy function $\phi(\lambda_1,\lambda_2,\lambda_3)$ occurs at critical values $\lambda_1^{cr},\lambda_2^{cr},\lambda_3^{cr}$ of the principal stretches $\lambda_1,\lambda_2,\lambda_3$ such that

$$\lambda_1^{cr}\lambda_2^{cr}\lambda_3^{cr}=1 \quad \text{and} \quad 0<\sum_{i=1}^{3} s_{i_*}^2(\lambda_1^{cr},\lambda_2^{cr},\lambda_3^{cr})<+\infty, \tag{13}$$

where

$$s_{i_*}(\lambda_1,\lambda_2,\lambda_3)\doteq\lim_{f_0\to 0+}\frac{\partial E}{\partial\lambda_i}(\lambda_1,\lambda_2,\lambda_3,f_0), \quad i=1,2,3. \tag{14}$$

Here, the function $E(\lambda_1,\lambda_2,\lambda_3,f_0)$ is defined by the initial-value problem

$$f_0\frac{\partial E}{\partial f_0}-E-\max_{\boldsymbol{\omega}(\boldsymbol{\xi})}\int_{|\boldsymbol{\xi}|=1}\frac{1}{4\pi}\left[\sum_{i=1}^{3}\frac{\partial E}{\partial\lambda_i}\xi_i\omega_i-\phi(\beta_1,\beta_2,\beta_3)\right]\mathrm{d}\boldsymbol{\xi}=0, \quad E(\lambda_1,\lambda_2,\lambda_3,1)=0, \tag{15}$$

where the maximizing vector $\boldsymbol{\omega}$ must satisfy the constraint (in component form)

$$\lambda_2\lambda_3\xi_1\omega_1(\boldsymbol{\xi})+\lambda_3\lambda_1\xi_2\omega_2(\boldsymbol{\xi})+\lambda_1\lambda_2\xi_3\omega_3(\boldsymbol{\xi})+\lambda_1\lambda_2\lambda_3-1=0 \tag{16}$$

and where β_1, β_2, β_3 denote the eigenvalues of $[(\mathbf{F}+\boldsymbol{\omega}\otimes\boldsymbol{\xi})^T(\mathbf{F}+\boldsymbol{\omega}\otimes\boldsymbol{\xi})]^{1/2}$ with $F_{ij}=\mathrm{diag}(\lambda_1,\lambda_2,\lambda_3)$. The corresponding critical principal Cauchy stresses t_1^{cr}, t_2^{cr}, t_3^{cr} at cavitation are given by

$$t_i^{cr}=\lambda_i^{cr}s_{i_*}(\lambda_1^{cr},\lambda_2^{cr},\lambda_3^{cr}), \quad i=1,2,3 \tag{17}$$

with no summation implied.

Note that condition (13) states quite simply that cavitation takes place at isochoric deformations ($\det\mathbf{F}=\lambda_1\lambda_2\lambda_3=1$) associated with non-zero bounded stresses, *irrespectively* of the type of incompressible stored-energy function ϕ being considered. By contrast, the critical stresses (17) at which cavitation occurs will depend critically on the specific choice of stored-energy function ϕ, as determined ultimately by the asymptotic solution to the initial-value problem (15) in the limit as $f_0\to 0+$. In this regard, we also note that the Hamilton–Jacobi equation $(15)_1$ depends only on three "space" variables (namely, $\lambda_1,\lambda_2,\lambda_3$), and therefore it is substantially easier to solve than the general Hamilton–Jacobi equation $(5)_1$ with nine "space" variables F_{ij} ($i,j=1,2,3$).

3. Application to Neo-Hookean materials

In the sequel, we employ the general formulation (13)–(17) for incompressible isotropic solids to work out a cavitation criterion for Neo-Hookean materials, with stored-energy function

$$\phi(\lambda_1,\lambda_2,\lambda_3)=\frac{\mu}{2}(\lambda_1^2+\lambda_2^2+\lambda_3^2-3), \tag{18}$$

under 3D loadings with arbitrary triaxiality; in expression (18), the positive material parameter μ denotes the shear modulus of the solid in its undeformed state. We begin (Section 3.1) by computing the asymptotic solution for the relevant total elastic energy E in the limit as $f_0\to 0+$, and then (Section 3.2) utilize this solution to write out the resulting cavitation criterion.

3.1. The total elastic energy E in the limit as $f_0\to 0+$

Within the context of the initial-value problem (15) — because the Neo-Hookean stored-energy function (18) depends on the principal stretches $\lambda_1,\lambda_2,\lambda_3$ only through the sum of their squares $\lambda_1^2+\lambda_2^2+\lambda_3^2$ — it proves convenient not to work with the principal stretches directly, but to work instead with the following combinations of stretches:

$$\Lambda_1=\frac{\lambda_1}{\lambda_2}, \quad \Lambda_2=\frac{\lambda_2}{\lambda_3}, \quad J=\lambda_1\lambda_2\lambda_3. \tag{19}$$

Thus, by making use of (19), defining $\hat{E}(\Lambda_1,\Lambda_2,J,f_0)\doteq E(\lambda_1,\lambda_2,\lambda_3,f_0)$, and carrying out the corresponding calculations, the initial-value problem (15) in this case reduces simply to the Hamilton–Jacobi equation

$$f_0\frac{\partial\hat{E}}{\partial f_0}-\hat{E}+(J-1)\frac{\partial\hat{E}}{\partial J}+\mu\mathcal{G}_0(\Lambda_1,\Lambda_2,J)+\frac{1}{J}\mathcal{G}_1(\Lambda_1,\Lambda_2)\frac{\partial\hat{E}}{\partial\Lambda_1}+\frac{1}{J}\mathcal{G}_2(\Lambda_1,\Lambda_2)\frac{\partial\hat{E}}{\partial\Lambda_2}$$

Please cite this article as: Lopez-Pamies, O., et al., Cavitation in elastomeric solids: II—Onset-of-cavitation surfaces for Neo-Hookean materials. J. Mech. Phys. Solids (2011), doi:10.1016/j.jmps.2011.04.016

$$+\frac{1}{\mu J^{2/3}}\mathcal{G}_3(\Lambda_1,\Lambda_2)\frac{\partial\hat{E}}{\partial\Lambda_1}\frac{\partial\hat{E}}{\partial\Lambda_2}+\frac{1}{\mu J^{2/3}}\mathcal{G}_4(\Lambda_1,\Lambda_2)\left(\frac{\partial\hat{E}}{\partial\Lambda_1}\right)^2+\frac{1}{\mu J^{2/3}}\mathcal{G}_5(\Lambda_1,\Lambda_2)\left(\frac{\partial\hat{E}}{\partial\Lambda_2}\right)^2=0 \tag{20}$$

subject to the initial condition

$$\hat{E}(\Lambda_1,\Lambda_2,J,1)=0. \tag{21}$$

The coefficients $\mathcal{G}_0$, $\mathcal{G}_1$, $\mathcal{G}_2$, $\mathcal{G}_3$, $\mathcal{G}_4$, $\mathcal{G}_5$ above are functions of their arguments given in explicit form by expressions (54) in Appendix A, where the key steps of the derivation of Eqs. (20) and (21) are also included. In passing it is interesting to note that the derivative $\partial\hat{E}/\partial J$, which serves to measure the homogenized response of the Neo-Hookean material with cavities to a change in volume, appears *linearly* in the pde (20). Thus, in spite of the fact that J is intrinsically a "space" variable, it can also be considered as a "time" variable in the Hamilton–Jacobi equation (20), a feature that may be exploited to simplify the construction of solutions for $\hat{E}$.

Having established Eqs. (20) and (21) for $\hat{E}$ for arbitrary values $f_0\in[0,1]$, our next objective is to compute their asymptotic solution in the limit as $f_0\to 0+$. To avoid loss of continuity, the pertinent derivations are given in Appendix B and here we merely record that the initial-value problem (20)–(21) admits the asymptotic solution

$$\hat{E}(\Lambda_1,\Lambda_2,J,f_0)=\hat{E}_0(\Lambda_1,\Lambda_2,J)+O(f_0^{1/3}) \tag{22}$$

with

$$\hat{E}_0(\Lambda_1,\Lambda_2,J)=\frac{\mu}{2}\left[J^{2/3}\frac{(\Lambda_1^2+1)\Lambda_2^2+1}{\Lambda_1^{2/3}\Lambda_2^{4/3}}-3\right]+\frac{3\mu}{2}\frac{(J-1)}{J^{1/3}}\Phi(\Lambda_1,\Lambda_2) \tag{23}$$

in the limit as $f_0\to 0+$. In this last expression, the function Φ is determined by the first-order nonlinear pde (75) subject to the initial condition (76). Unfortunately, this initial-value problem does not admit a closed-form solution, but it can, however, readily be solved numerically. Fig. 1(a) shows plots of such a solution over a large range of deformations ($0<\Lambda_1\le 10$ and $0<\Lambda_2\le 10$). A few properties worth remarking about the function Φ, which are easily recognizable from Fig. 1(a), are that it is bounded from above by 1 and from below by 0:

$$0<\Phi(\Lambda_1,\Lambda_2)\le 1\quad\forall\ \Lambda_1,\Lambda_2>0, \tag{24}$$

that its global maximum, which happens to also correspond to its only local maximum, is attained at $\Lambda_1=\Lambda_2=1$:

$$\max_{\Lambda_1,\Lambda_2}\{\Phi(\Lambda_1,\Lambda_2)\}=\Phi(1,1)=1, \tag{25}$$

and that it tends to zero, albeit slowly, as the deformation becomes infinitely large:

$$\Phi(\Lambda_1,\Lambda_2)\to 0\quad\text{as }\Lambda_1\to 0,+\infty\text{ and/or }\Lambda_2\to 0,+\infty. \tag{26}$$

The proof of relations (24)–(26) together with relevant comments on the numerical computation of Φ are given in Appendix C.

At this stage, it is a simple matter to rewrite the asymptotic solution (22) directly in terms of the principal stretches $\lambda_1,\lambda_2,\lambda_3$, as ultimately required in the onset-of-cavitation conditions (14), (13), and (17). Indeed, by making use of the definition $\hat{E}(\Lambda_1,\Lambda_2,J,f_0)\doteq E(\lambda_1,\lambda_2,\lambda_3,f_0)$ and relations (19), we readily have that the asymptotic solution in the limit as $f_0\to 0+$ to the initial-value problem (15) for E when specialized to Neo-Hookean materials (18) is given by

$$E(\lambda_1,\lambda_2,\lambda_3,f_0)=E_0(\lambda_1,\lambda_2,\lambda_3)+O(f_0^{1/3}) \tag{27}$$

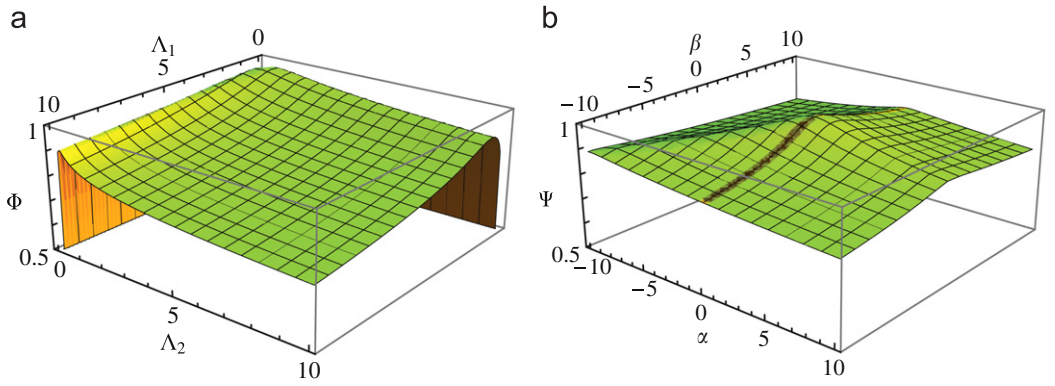

Fig. 1. (a) Plot of the solution to the initial-value problem (75)–(76) for the function $\Phi(\Lambda_1,\Lambda_2)$, for a large range of deformations Λ_1 and Λ_2. Note that $\Phi(1,1)=1$, that $\Phi(\Lambda_1,\Lambda_2)$ decreases monotonically as Λ_1 and Λ_2 deviate from 1 in any radial path, and that $0<\Phi(\Lambda_1,\Lambda_2)\le 1$. (b) Plot of the function $\Psi(\alpha,\beta)$ defined by (32), for a large range of values of its arguments α and β. Similar to the behavior of Φ, note that $\Psi(0,0)=1$, that $\Psi(\alpha,\beta)$ decreases monotonically as α and β deviate from 0 in any radial path, and that $0<\Psi(\alpha,\beta)\le 1$.

Please cite this article as: Lopez-Pamies, O., et al., Cavitation in elastomeric solids: II—Onset-of-cavitation surfaces for Neo-Hookean materials. J. Mech. Phys. Solids (2011), doi:10.1016/j.jmps.2011.04.016

with

$$E_0(\lambda_1,\lambda_2,\lambda_3)=\frac{\mu}{2}(\lambda_1^2+\lambda_2^2+\lambda_3^2-3)+\frac{3\mu}{2}\frac{(\lambda_1\lambda_2\lambda_3-1)}{(\lambda_1\lambda_2\lambda_3)^{1/3}}\Phi\left(\frac{\lambda_1}{\lambda_2},\frac{\lambda_2}{\lambda_3}\right), \tag{28}$$

where it is re-emphasized that the function Φ is defined by the pde (75) with initial condition (76), satisfies properties (24)–(26), and is plotted in Fig. 1(a).

Some remarks regarding the result (27) are now in order. For isochoric loadings when $\lambda_1\lambda_2\lambda_3=1$, the leading order term (28) of the total elastic energy (27) reduces identically to the energy (18) of a Neo-Hookean material. For non-isochoric loadings when $\lambda_1\lambda_2\lambda_3\neq 1$, on the other hand, the energy (28) differs drastically from (18), especially in that it is compressible (i.e., E_0 remains finite for loadings with $\lambda_1\lambda_2\lambda_3\neq 1$, as opposed to the Neo-Hookean energy which becomes unbounded). Hence, according to the solution (27), the presence of zero-volume defects *does not* affect the mechanical response of Neo-Hookean materials under volume-preserving loading conditions, but it *does* drastically affect it for any other type of loading. This is consistent with the fact that — because of the incompressibility of the Neo-Hookean material — pre-existing defects of zero initial volume remain of zero volume under any loading with $\lambda_1\lambda_2\lambda_3=1$, but they grow to finite volume under loadings with $\lambda_1\lambda_2\lambda_3>1$, thus resulting in a homogenized response that is compressible. In other words, the homogenized response of a Neo-Hookean material that contains a random isotropic distribution of zero-volume vacuous defects — as characterized by (28) — is *identical* to the response of a Neo-Hookean material without defects for loadings for which the defects remain of zero volume. By contrast, for loadings for which the defects grow to finite sizes — that is, at and beyond cavitation — the homogenized response of a Neo-Hookean material with defects becomes radically different from that of a defect-free Neo-Hookean material.

3.2. Cavitation criterion

We are now in a position to make use of the asymptotic result (27) in expressions (14), (13), and (17) to finally determine a cavitation criterion for Neo-Hookean materials under 3D loading conditions with arbitrary triaxiality. Thus, after substituting (27) in (14), it is straightforward to deduce that cavitation occurs in Neo-Hookean materials at critical values $\lambda_1^{cr},\lambda_2^{cr},\lambda_3^{cr}$ of the principal stretches $\lambda_1,\lambda_2,\lambda_3$ such that

$$\lambda_1^{cr}\lambda_2^{cr}\lambda_3^{cr}=1, \tag{29}$$

and at critical values t_1^{cr}, t_2^{cr}, t_3^{cr} of the principal Cauchy stresses t_1, t_2, t_3 given by

$$t_i^{cr}=\lambda_i^{cr}\frac{\partial E_0}{\partial\lambda_i}(\lambda_1^{cr},\lambda_2^{cr},\lambda_3^{cr})=\mu(\lambda_i^{cr})^2+\frac{3\mu}{2}\Phi\left(\frac{\lambda_1^{cr}}{\lambda_2^{cr}},\frac{\lambda_2^{cr}}{\lambda_3^{cr}}\right),\quad i=1,2,3 \tag{30}$$

with no summation implied. Condition (29) states that cavitation occurs at *isochoric deformations*. This is necessarily the case for any incompressible material (not just Neo-Hookean) that does cavitate, as already noted in the broader context of Section 2. The more insightful conditions (30) reveal that cavitation can only occur when all three principal stresses are *tensile*, since $\mu>0$, $\lambda_i^{cr}>0$, and $\Phi>0$ so that $t_i^{cr}>0$ ($i=1,2,3$). More specifically, conditions (30) correspond to the parametric equations (with parameters $\lambda_1^{cr}>0$, $\lambda_2^{cr}>0$, $\lambda_3^{cr}>0$ satisfying the constraint $\lambda_1^{cr}\lambda_2^{cr}\lambda_3^{cr}=1$) of a surface, S say, in the first octant of the (t_1,t_2,t_3)-space. We shall refer to such a surface as *onset-of-cavitation surface*. It is possible to eliminate the parameters λ_1^{cr}, λ_2^{cr}, and λ_3^{cr} from (30) to obtain an expression for S solely in terms of the stresses. The result reads as follows:

$$\begin{aligned}S(t_1,t_2,t_3)=&\,8t_1t_2t_3-12\mu(t_1t_2+t_1t_3+t_2t_3)\Psi(t_2-t_1,t_3-t_1)+18\mu^2(t_1+t_2+t_3)\Psi^2(t_2-t_1,t_3-t_1)\\&-27\mu^3\Psi^3(t_2-t_1,t_3-t_1)-8\mu^3=0,\end{aligned} \tag{31}$$

where, to ease notation, the superscript "cr" has been dropped and

$$\Psi(\alpha,\beta)\doteq\Phi\left(\sqrt{\Xi(\alpha,\beta)},\sqrt{\frac{-\Xi(\alpha,\beta)\alpha^3}{(\Xi(\alpha,\beta)-1)^3\mu^3}}\right), \tag{32}$$

where

$$\Xi(\alpha,\beta)=1+\frac{(\beta-\alpha)\alpha^2}{3\mu^3}\pm\left[\frac{C(\alpha,\beta)}{[\sqrt{A(\alpha,\beta)}\pm B(\alpha,\beta)]^{1/3}}-\frac{\alpha}{\mu}[\sqrt{A(\alpha,\beta)}\pm B(\alpha,\beta)]^{1/3}\right] \tag{33}$$

with

$$\begin{aligned}A(\alpha,\beta)&=\frac{1}{108\mu^6}[-\alpha^2\beta^2(\alpha-\beta)^2-2\mu^3(\alpha-2\beta)(2\alpha-\beta)(\alpha+\beta)+27\mu^6],\\B(\alpha,\beta)&=\frac{1}{54\mu^6}[2\alpha^3(\alpha-\beta)^3-9\mu^3\alpha(2\alpha^2-3\alpha\beta+\beta^2)+27\mu^6],\\C(\alpha,\beta)&=-\frac{1}{9\mu^5}\alpha[\alpha^2(\alpha-\beta)^2-3\mu^3(2\alpha-\beta)].\end{aligned} \tag{34}$$

Please cite this article as: Lopez-Pamies, O., et al., Cavitation in elastomeric solids: II—Onset-of-cavitation surfaces for Neo-Hookean materials. J. Mech. Phys. Solids (2011), doi:10.1016/j.jmps.2011.04.016

The root (positive "+" or negative "−") that must be selected in expression (33) is the one that renders $\Xi(\alpha,\beta)\geq 1$ if $\alpha\leq 0$ and $\Xi(\alpha,\beta)<1$ if $\alpha>0$. It is also emphasized that only the root with $t_i>0$ ($i=1,2,3$) must be selected in (31), as dictated by the parametric expressions (30). Note further that the function Ψ is nothing more than a composite function of Φ (see Appendix C). It then follows from the properties (24)–(26) of Φ that Ψ is bounded from above by 1 and from below by 0:

$$0<\Psi(\alpha,\beta)\leq 1 \quad \forall \alpha,\beta\in\mathbb{R}, \tag{35}$$

that its global maximum corresponds to its only local maximum and is attained at $\alpha=\beta=0$:

$$\max_{\alpha,\beta}\{\Psi(\alpha,\beta)\}=\Psi(0,0)=1, \tag{36}$$

and that it slowly tends to zero as its arguments become infinitely large:

$$\Psi(\alpha,\beta)\to 0 \quad \text{as } \alpha\to\pm\infty \text{ and/or } \beta\to\pm\infty. \tag{37}$$

For completeness, Fig. 1(b) shows a plot of Ψ over a large range of values of its arguments ($-10<\alpha<10$ and $-10<\beta<10$).

To better reveal the role of load triaxiality in the onset of cavitation in Neo-Hookean materials, it proves convenient for later use to rewrite expression (31) in terms of the following alternative stress quantities:

$$\sigma_m\doteq\tfrac{1}{3}(t_1+t_2+t_3), \quad \tau_1\doteq t_2-t_1, \quad \tau_2\doteq t_3-t_1. \tag{38}$$

Here, the mean stress σ_m provides a measure of the hydrostatic loading in a given state of stress, while τ_1 and τ_2 provide a measure of the shear loading. Larger values of $|\tau_1|$ and $|\tau_2|$ correspond to lower load triaxiality and represent a greater departure from a state of pure hydrostatic stress. Thus, in the space of stress measures (38), the onset-of-cavitation surface (31) takes the form

$$\begin{aligned}\mathcal{S}(\sigma_m,\tau_1,\tau_2)=&\,8(3\sigma_m-\tau_1-\tau_2)(3\sigma_m+2\tau_1-\tau_2)(3\sigma_m+2\tau_2-\tau_1)-729\mu^3\Psi^3(\tau_1,\tau_2)+1458\mu^2\sigma_m\Psi^2(\tau_1,\tau_2)\\&-108\mu(9\sigma_m^2-\tau_1^2-\tau_2^2+\tau_1\tau_2)\Psi(\tau_1,\tau_2)-216\mu^3=0,\end{aligned} \tag{39}$$

where, according to (30), we note that only the root with $\sigma_m>1/3(\tau_1+\tau_2)$, $\sigma_m>1/3(\tau_1-2\tau_2)$, and $\sigma_m>1/3(\tau_2-2\tau_1)$ must be selected in this expression. There are two limiting cases worth spelling out from the onset-of-cavitation surface (39). The first one corresponds to the case of axisymmetric loading conditions when two of the principal stresses are the same, $t_3=t_2$ say so that $\tau_2=\tau_1$. In this case, (39) collapses to an onset-of-cavitation curve $\mathcal{C}(\sigma_m,\tau_1)$ given by

$$\mathcal{C}(\sigma_m,\tau_1)=\mathcal{S}(\sigma_m,\tau_1,\tau_1)=\sigma_m-\frac{3\mu}{2}\Psi(\tau_1,\tau_2)-\frac{2^{4/3}\tau_1^2+\left(4\tau_1^3+54\mu^3+6\sqrt{81\mu^6+12\mu^3\tau_1^3}\right)^{2/3}}{6\left(2\tau_1^3+27\mu^3+3\sqrt{81\mu^6+12\mu^3\tau_1^3}\right)^{1/3}}=0. \tag{40}$$

For the case when all three principal stresses are the same, so that the shear stresses $\tau_1=\tau_2=0$, expression (39) reduces further to an onset-of-cavitation point $\mathcal{P}(\sigma_m)$ that reads as

$$\mathcal{P}(\sigma_m)=\mathcal{S}(\sigma_m,0,0)=\sigma_m-\frac{5\mu}{2}=0 \tag{41}$$

and provides the value of the critical Cauchy pressure at which cavitation occurs under pure hydrostatic loading. Note that (41) agrees identically with the classical result of Gent and Lindley (*cf.* Gent and Lindley, 1959, Eq. (3)) and of Ball (*cf.* Ball, 1982, Eq. (5.66)) for the radially symmetric cavitation of a Neo-Hookean material, as expected from the general connections established in Section 5 of Part I.

Plots and a detailed discussion of the above onset-of-cavitation surfaces — including comparisons with the finite-element results to be derived in the next section, as well as with earlier results available from the literature — are deferred to Section 5.

4. Finite-element simulations for the onset of cavitation in Neo-Hookean materials under multi-axial loading

In order to compare the above theoretical results with a separate solution, a 3D finite-element (FE) model is utilized (Nakamura and Lopez-Pamies, submitted for publication). Here the critical loads at which a *single spherical* cavity of infinitesimal size, embedded in a block of Neo-Hookean material subjected to general loading conditions, suddenly grows to finite size are computed. The comparison between these onset-of-cavitation results for an *isolated spherical defect* with the results of the preceding section for an *isotropic distribution of defects* will shed some light on the importance of interactions among defects in the occurrence of cavitation in elastomeric solids.

4.1. The FE model

Without loss of generality, we consider the case in which the cavity is located at the center of an initially cubic Neo-Hookean block. The pre-existing cavity is set to have an initial volume fraction[4] of $f_0=\pi/6\times 10^{-9}\approx 0.5\times 10^{-9}$, corresponding to a cavity

[4] A parametric study of the problem with decreasing values of initial volume fraction of cavity in the range $10^{-6}\leq f_0\leq 10^{-12}$ indicates that $f_0=\pi/6\times 10^{-9}$ is sufficiently small to be representative of an actual infinitesimal cavity with $f_0\to 0+$, thus supporting this choice.

Please cite this article as: Lopez-Pamies, O., et al., Cavitation in elastomeric solids: II—Onset-of-cavitation surfaces for Neo-Hookean materials. J. Mech. Phys. Solids (2011), doi:10.1016/j.jmps.2011.04.016

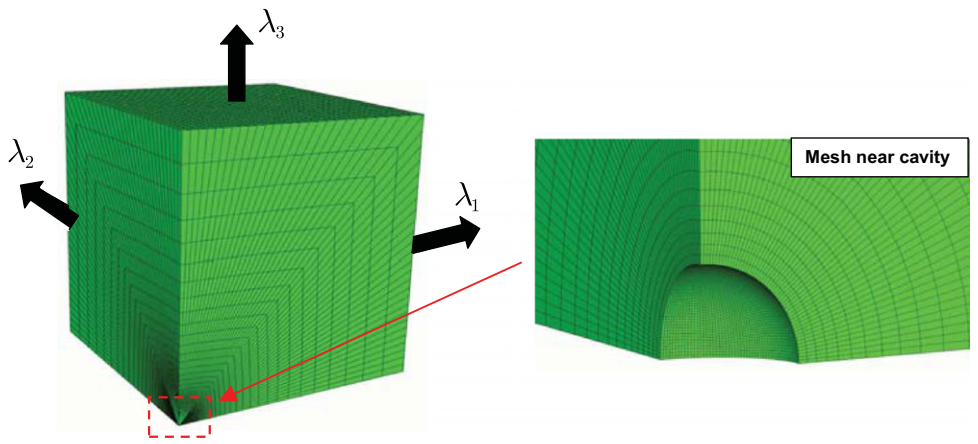

Fig. 2. Finite-element model — in the undeformed configuration — of a small vacuous spherical cavity located at the center of a cubic block. The outer boundary of the cube is subjected to affine stretches $\lambda_1,\lambda_2,\lambda_3$ aligned with the three principal axes of the cube.

of radius 1 in a cube of side 2000. The symmetry of the problem allows to perform the calculations in just one octant of the cube. A mesh generator code is used to construct the 3D geometry as shown in Fig. 2. Here the mesh is designed so that the small elements are placed near the cavity at uniform angular intervals of 2.25°, while the radial element sizes are gradually increased toward the outer boundary. In all, the mesh consists of 64,800 8-node brick elements (with 1200 elements in each radial plane and 54 layers in the radial direction[5]). The computations are carried using the FE code ABAQUS with hybrid[6] 8-node linear elements (C3D8H) due to the full incompressibility of the material; it is appropriate to remark that higher order elements (e.g., quadratic 20-node elements) are not suitable for the present problem because of the extremely large deformations involved. The inner boundary of the cavity is set to be stress free, while the outer boundary of the cube is subjected to affine stretches $\lambda_1,\lambda_2,\lambda_3$ aligned with the three principal axes of the cube (see Fig. 2). Consistent with the notation of the previous section, the affine principal Cauchy stresses resulting on the outer boundary of the cube are similarly denoted by t_1,t_2,t_3.

4.2. Computation of the onset-of-cavitation surface

Because the size of the cavity in the FE model is necessarily *finite*, its sudden growth signaling cavitation does *not* occur abruptly at a single load, but instead it occurs over a small range of loads. This behavior is illustrated in Fig. 3(a) for the case of hydrostatic loading ($\lambda_1=\lambda_2=\lambda_3\geq 1$), where the normalized volume fraction of cavity f/f_0 is plotted versus the mean (hydrostatic) stress[7] σ_m on the outer boundary of the cube. The figure clearly shows that the volume fraction of the cavity f remains unchanged in the order of $f_0=\pi/6\times 10^{-9}$ until the far-field hydrostatic stress approaches the value of 2.5μ, just before which the cavity begins to grow very rapidly but *smoothly*. For definiteness, in this work we shall consider that whenever the volume fraction of cavity in the FE model increases five orders of magnitude, reaching the critical value

$$f_{cr}=10^5\times f_0=\frac{\pi}{6}\times 10^{-4}, \tag{42}$$

cavitation ensues. In this regard, it should be noted that using different criteria — such as a four-orders-of-magnitude increase $f_{cr}=10^4\times f_0$ or a six-orders-of-magnitude increase $f_{cr}=10^6\times f_0$ — leads to somewhat different values for the critical loads at which cavitation occurs, yet the qualitative character of the results remains unaltered. As a reference, we also note that the criterion (42) leads to a critical pressure of $\sigma_m=2.46\mu$ for the onset of cavitation in a Neo-Hookean material under hydrostatic loading, in comparison to the classical result of $\sigma_m=2.5\mu$ based on the solution for $f_0\to 0+$.

Having set the cavitation criterion (42) for the FE model, we now turn to the computation of the critical loads at which cavitation occurs. Here, we utilize the incompressibility of the Neo-Hookean material effectively to determine these loads. Since the volume fraction of the cavity is related to the applied stretches via the kinematical expression $\lambda_1\lambda_2\lambda_3=(1-f_0)/(1-f)$, it can be deduced from (42) that cavitation occurs in the FE model at critical values $\lambda_1^{cr},\lambda_2^{cr},\lambda_3^{cr}$ of the applied stretches $\lambda_1,\lambda_2,\lambda_3$ such that

$$\lambda_1^{cr}\lambda_2^{cr}\lambda_3^{cr}=J_{cr}\doteq\frac{1-f_0}{1-f_{cr}}=\frac{1-\frac{\pi}{6}\times 10^{-9}}{1-\frac{\pi}{6}\times 10^{-4}}\approx 1.0000523621. \tag{43}$$

[5] This discretization was selected after various mesh refinements were tried to assess the accuracy.
[6] These elements treat both the displacement field and the hydrostatic component of the stress as interpolated basic variables.
[7] Throughout this paper, all stress quantities shown in plots are normalized by the shear modulus μ of the Neo-Hookean material.

Please cite this article as: Lopez-Pamies, O., et al., Cavitation in elastomeric solids: II—Onset-of-cavitation surfaces for Neo-Hookean materials. J. Mech. Phys. Solids (2011), doi:10.1016/j.jmps.2011.04.016

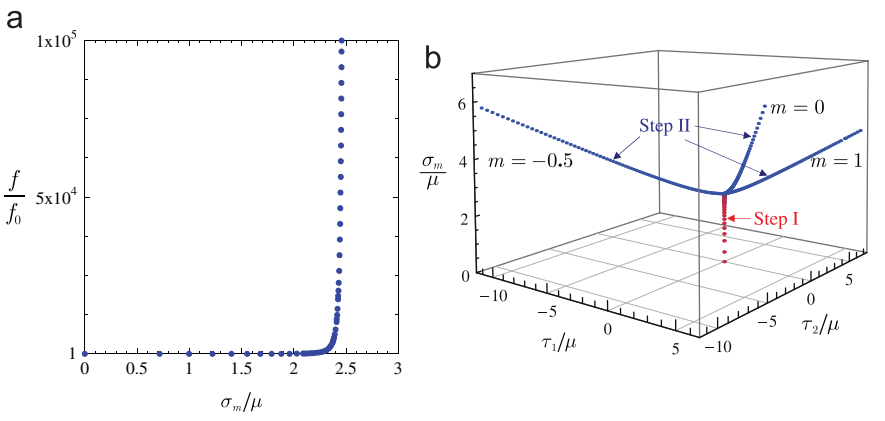

Fig. 3. (a) Increase in the volume fraction f of cavity in the FE model, as a function of the far-field mean (hydrostatic) stress σ_m, for the case of hydrostatic loading with $\lambda_1=\lambda_2=\lambda_3\geq 1$. (b) FE solutions for the hydrostatic stress σ_m versus the shear stresses τ_1 and τ_2 that result on the outer boundary of the cube by marching along the two-step loading process (44)–(45) for three values of the parameter m. The stresses associated with Step II correspond to the critical stresses at which cavitation ensues.

The critical values t_1^{cr}, t_2^{cr}, t_3^{cr} of the corresponding principal Cauchy stresses t_1, t_2, t_3 on the outer boundary of the cube can then be found by marching along (starting at $\lambda_1=\lambda_2=\lambda_3=1$) volume-increasing loading paths in $(\lambda_1,\lambda_2,\lambda_3)$-space until the product $\lambda_1\lambda_2\lambda_3$ reaches the value (43). An alternative, more efficient strategy is to first subject the cube to hydrostatic loading until condition (43) is reached, and then vary the ratios of the stretches λ_1/λ_2 and λ_2/λ_3 while keeping their product fixed at the cavitated state $\lambda_1\lambda_2\lambda_3=J_{cr}$ in such a way that the critical stresses t_1^{cr}, t_2^{cr}, t_3^{cr} are computed continuously along the loading path. A convenient parameterization of this two-step loading process is as follows:

$$\text{Step I}: \lambda_1=\lambda_2=\lambda_3=\lambda \quad \text{for } 1\leq\lambda\leq J_{cr}^{1/3} \tag{44}$$

and

$$\text{Step II}: \lambda_1=\lambda, \quad \lambda_2=\lambda^m, \quad \lambda_3=J_{cr}\lambda^{-(1+m)} \text{ for } \lambda>J_{cr}^{1/3}, \tag{45}$$

where λ is a monotonically increasing load parameter that takes the value of 1 in the undeformed configuration and $m\in\mathbb{R}$, but because of symmetry it actually suffices to restrict attention to $m\in[-0.5,1]$. Fig. 3(b) shows FE solutions for the principal Cauchy stresses t_1, t_2, t_3 on the outer boundary of the cube that result by marching along the above two-step loading process for the cases of $m=-0.5,0$, and 1; for each m in Step II, the computation is restarted from the hydrostatic loading results of Step I. For consistency with the next section, the results are plotted in terms of the hydrostatic stress $\sigma_m=1/3(t_1+t_2+t_3)$ as a function of the shear stresses $\tau_1=t_2-t_1$ and $\tau_2=t_3-t_1$. Note that the stresses associated with Step II of the loading process correspond precisely to the critical stresses at which cavitation ensues. The entire onset-of-cavitation surface can then be constructed by simply carrying out more calculations for various values of $m\in[-0.5,1]$.

5. Onset-of-cavitation surfaces and discussion

We present here results of the onset-of-cavitation surfaces worked out in Sections 3 and 4, as well as of some earlier results available in the literature. In the first set of plots, we focus on the case of axisymmetric loading conditions. As it will become apparent below, this special case serves to illustrate in a "two-dimensional" setting all the main effects that load triaxiality — namely, the departure from pure hydrostatic loading — has on the onset of cavitation in Neo-Hookean materials. The second set of plots pertains to the entire onset-of-cavitation surfaces for general loading conditions.

5.1. Axisymmetric loading

Fig. 4 shows plots for the hydrostatic stress σ_m and shear stress τ_1 at which cavitation ensues in Neo-Hookean materials under axisymmetric loading conditions with $\tau_2=\tau_1$ (recall the definition (38)). The solid line corresponds to the theoretical result (40) derived in Section 3, while the solid circles denote the FE results generated in Section 4. The figure also includes the variational approximation (dashed line) of Hou and Abeyaratne (1992) and the earlier numerical results (triangles) of Chang et al. (1993) based on an allegedly equivalent[8] 2D axisymmetric FE model.

A key observation from Fig. 4 is that cavitation occurs only at states of axisymmetric stress for which the hydrostatic part σ_m is *tensile*, in accordance with experiments. For all four results, the critical value of σ_m is lowest for purely hydrostatic loading when $\tau_1=0$, and increases significantly and monotonically as the shear stress τ_1 deviates from

[8] Chang et al. (1993) examined the problem of a pressurized cavity in a cylindrical block under uniaxial tension and considered it as equivalent to the problem of a vacuous cavity in a cylindrical block under multi-axial tension.

Please cite this article as: Lopez-Pamies, O., et al., Cavitation in elastomeric solids: II—Onset-of-cavitation surfaces for Neo-Hookean materials. J. Mech. Phys. Solids (2011), doi:10.1016/j.jmps.2011.04.016

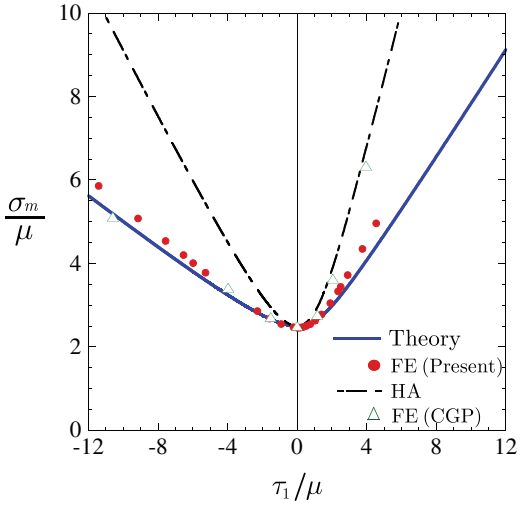

Fig. 4. Onset-of-cavitation curves for Neo-Hookean materials under axisymmetric loading with $\tau_2=\tau_1$ in the space of (σ_m,τ_1)-stress. The solid line corresponds to the theoretical result (40), the solid circles correspond to the FE results generated in Section 4, the dashed line indicates the variational approximation of Hou and Abeyaratne (1992), and the triangles denote the earlier FE results of Chang et al. (1993).

zero—that is, as the load triaxiality decreases. Note in particular that the critical σ_m increases faster for loadings with $\tau_1>0$, which correspond to the case when the two principal Cauchy stresses that are equal (t_2 and t_3 in this case) are greater than the other principal Cauchy stress (t_1 in this case).

Another key observation from Fig. 4 is that the FE cavitation results generated in Section 4 are in fairly good agreement with the theoretical onset-of-cavitation curve (40). This is a remarkable connection given that the FE results are based on the growth of a *single spherical cavity*, while the theoretical result (40) is based on the growth of an *isotropic distribution of cavities*. This agreement thus suggests that the interaction among cavities may not play an important role in the onset of cavitation in elastomeric solids. Further evidence supporting this possibility has been provided by the recent work of Xu and Henao (in press), who have shown — in the context of a class of 2D compressible isotropic elastic solids — that the critical load at which cavitation ensues based on the growth of an isolated defect is essentially the same as that based on the growth of two neighboring defects. This issue is worth of further study in more general material systems.

Finally, we remark from Fig. 4 that the variational approximation of Hou and Abeyaratne (1992) has the same qualitative behavior as the theoretical result (40). Quantitatively, it agrees with (40) for purely hydrostatic loading ($\tau_1=0$), but predicts much larger critical stresses for the onset of cavitation as the shear stress τ_1 deviates from 0. This behavior is consistent with the fact that their approximation was constructed by making use of a kinematically admissible trial field in certain energy minimization problem, thus leading to overpredictions for the actual critical stresses at cavitation.[9] We also remark that the FE results of Chang et al. (1993) are in agreement with our FE results — and therefore with the theoretical result (40) — except for loadings with large positive shear stress τ_1. It should be noted, however, that the equivalency between the two FE approaches remains to be verified.

5.2. General loading

Fig. 5(a) displays the onset-of-cavitation surface (39) for Neo-Hookean materials under 3D loading conditions with arbitrary triaxiality. The surface is plotted in terms of the hydrostatic stress σ_m as a function of the shear stresses τ_1 and τ_2 at which cavitation ensues. The overall features of the surface are seen to be identical to those of the onset-of-cavitation curve shown in Fig. 4 for the case of axisymmetric loading. Namely, cavitation occurs only at states of stress for which the hydrostatic part σ_m is *tensile*. Moreover, the critical value of σ_m is lowest for purely hydrostatic loading when $\tau_1=\tau_2=0$, and increases significantly and monotonically as the shear stresses τ_1 and τ_2 deviate from zero in any radial path—that is, as the load triaxiality decreases. Making use of an approximate linear-comparison technique in the corresponding two-dimensional problem, Lopez-Pamies (2009) found this same trend of increasing σ_m with decreasing load triaxiality for *compressible* Neo-Hookean materials. However, he also found that other classes of *compressible* materials exhibit the exact opposite trend (see Section 5.2, Lopez-Pamies, 2009). The question arises then as to whether the "exact" theory proposed in Part I confirms such trends. This issue, which can have strong practical implications, will be investigated in future work.

Fig. 5(b) compares the theoretical surface (39) with the onset-of-cavitation surface generated from the FE results of Section 4; for clarity of presentation, only results in the quadrant of negative shear stresses τ_1 and τ_2 are included in the

[9] Specifically, their result constitutes a rigorous upper bound for the critical far-field stresses at which a single vacuous spherical cavity embedded in an infinite Neo-Hookean medium suddenly grows unbounded.

Please cite this article as: Lopez-Pamies, O., et al., Cavitation in elastomeric solids: II—Onset-of-cavitation surfaces for Neo-Hookean materials. J. Mech. Phys. Solids (2011), doi:10.1016/j.jmps.2011.04.016

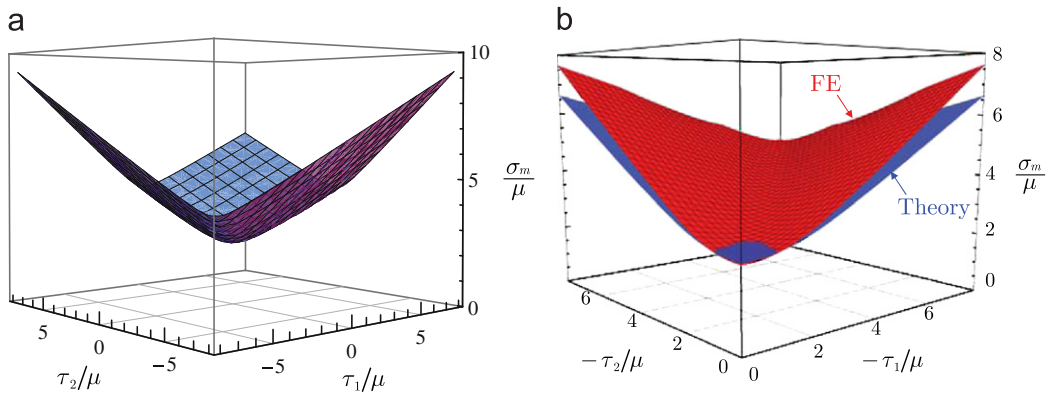

Fig. 5. (a) 3D plot of the theoretical onset-of-cavitation surface (39) for Neo-Hookean materials in the space of (σ_m,τ_1,τ_2)-stress. (b) Comparison of (39) with the onset-of-cavitation surface generated from the FE results of Section 4.

figure. The FE surface is seen to be identical in form to the theoretical surface. The quantitative agreement is also remarkably good—in spite of the fact, again, that the FE results are based on the growth of a *single spherical cavity*, while the theoretical result (40) is based on the growth of an *isotropic distribution of cavities*. Much like in the case of axisymmetric loading shown in Fig. 4 (which corresponds to the line $\tau_2=\tau_1$ in this plot) the FE results are seen to predict similar, but progressively higher hydrostatic stresses as the load triaxiality decreases (i.e., as τ_1 and τ_2 deviate from zero), for the onset of cavitation in Neo-Hookean materials.

In summary, the above results indicate that Neo-Hookean solids significantly improve their stability — in the sense that cavitation takes place at larger mean (hydrostatic) stresses — with decreasing load triaxiality. This has strong practical implications. For instance, in the contexts of filled elastomers (Gent and Park, 1984; Cho et al., 1987; Moraleda et al., 2009; Michel et al., 2010) and structures bonded by soft adhesives (Creton and Hooker, 2001), the regions surrounding the inherent soft/stiff interfaces are known to develop high stress triaxialities and therefore are prone to cavitation. Yet the stress states in these regions are *not* purely hydrostatic but do involve sizable shear stresses. Predictions based upon radially symmetric cavitation ignoring the effect of shear stresses in these material systems may then result in substantial errors, and may even lead to incorrect conclusions. In the context of rubber-toughened polymers (Cheng et al., 1995; Steenbrink and Van der Giessen, 1999), the underlying rubber particles also develop states of high — but not purely — hydrostatic stress. Ignoring the effect of shear stresses on the onset of cavitation in this case may also lead to incorrect conclusions.

6. An approximate *closed-form* cavitation criterion for Neo-Hookean materials

The cavitation criterion (31) requires knowledge of the function Ψ defined by (32), which ultimately amounts to solving *numerically* the pde (75) subject to the initial condition (76). In this section, we propose an *approximate* criterion which is *closed form* and very close to the exact criterion (31).

The approximation is based on the observation that the function Ψ takes the value 1 for purely hydrostatic loading and decays slowly to zero with decreasing load triaxiality, as described by the properties (35)–(37) and illustrated graphically in Fig. 1(b). Thus, we can generate an approximate criterion that agrees exactly with the exact criterion (31) at the hydrostatic point by simply taking the function Ψ equal to 1 in (31). The result is given by

$$S_B(t_1,t_2,t_3)=8t_1t_2t_3-12\mu(t_1t_2+t_1t_3+t_2t_3)+18\mu^2(t_1+t_2+t_3)-35\mu^3=0, \tag{46}$$

where only the root with $t_i>0$ $(i=1,2,3)$ ought to be selected. In the space of stress measures (38), this approximate criterion takes the form

$$\mathcal{S}_B(\sigma_m,\tau_1,\tau_2)=8(3\sigma_m-\tau_1-\tau_2)(3\sigma_m+2\tau_1-\tau_2)(3\sigma_m+2\tau_2-\tau_1)-108\mu(9\sigma_m^2-\tau_1^2-\tau_2^2+\tau_1\tau_2)+1458\mu^2\sigma_m-945\mu^3=0, \tag{47}$$

where only the root with $\sigma_m>3\mu/2+1/3(\tau_1+\tau_2)$, $\sigma_m>3\mu/2+1/3(\tau_1-2\tau_2)$, and $\sigma_m>3\mu/2+1/3(\tau_2-2\tau_1)$ ought to be selected. It is easy to verify that these surfaces contain the hydrostatic point (41).

Fig. 6 provides comparisons between the exact surface (39) — shown in solid lines — and its closed-form approximation (47) — shown in dotted lines — in the space of (σ_m,τ_1,τ_2)-stress. Part (a) shows plots for axisymmetric loading with $\tau_2=\tau_1$, in which case the approximate surface (47) reduces to the curve

$$\mathcal{S}_B(\sigma_m,\tau_1,\tau_1)=\sigma_m-\frac{3\mu}{2}-\frac{2^{4/3}\tau_1^2+\left(4\tau_1^3+54\mu^3+6\sqrt{81\mu^6+12\mu^3\tau_1^3}\right)^{2/3}}{6\left(2\tau_1^3+27\mu^3+3\sqrt{81\mu^6+12\mu^3\tau_1^3}\right)^{1/3}}=0. \tag{48}$$

Please cite this article as: Lopez-Pamies, O., et al., Cavitation in elastomeric solids: II—Onset-of-cavitation surfaces for Neo-Hookean materials. J. Mech. Phys. Solids (2011), doi:10.1016/j.jmps.2011.04.016

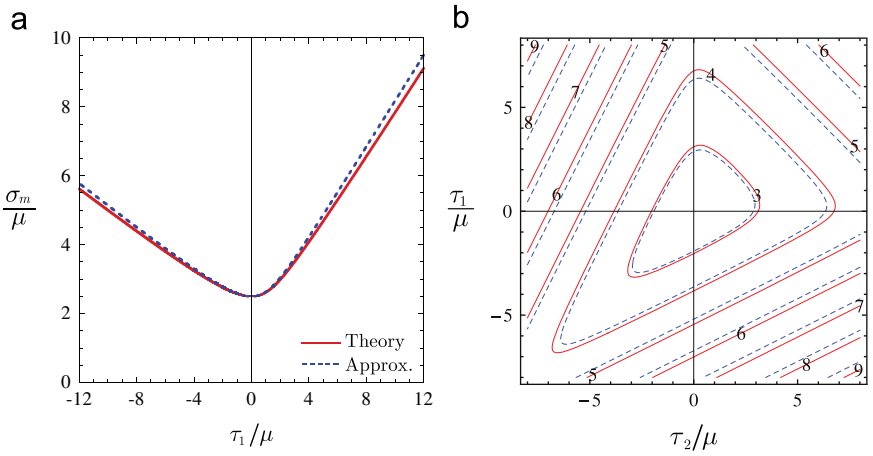

Fig. 6. Comparisons between the exact onset-of-cavitation surface (39) and its closed-form approximation (47). Part (a) shows results for the hydrostatic stress σ_m as a function of the shear stress τ_1 for the special case of axisymmetric loading with $\tau_2=\tau_1$, while part (b) shows contour lines of σ_m as a function of τ_1 and τ_2 for general loading conditions. In both parts, the solid lines correspond to the exact surface (39) and the dashed lines to its closed-form approximation (47).

The comparisons show that, indeed, the approximate curve agrees exactly with the exact curve at the hydrostatic point ($\tau_1=0$) and remains remarkably close to the exact curve over a large range of shear stresses τ_1. Comparisons for general loading conditions are provided in part (b). This figure shows contour lines of hydrostatic stress σ_m in the space of shear stresses (τ_1,τ_2). Once again, the approximate surface is seen to reproduce remarkably accurately the exact surface for the entire large range of shear stresses τ_1 and τ_2 considered.

Fig. 6 also shows that the approximate surface always lies "outside" the exact surface (relative to the origin). In fact, the approximate surfaces (46) and (47) can be shown to be rigorous outer bounds for the corresponding exact surfaces (31) and (39). To see this, note that in view of the relations (29), (30), and (38) any stress state lying on the exact surface (39) can be written parametrically as

$$\tau_1=\mu(\lambda_2^2-\lambda_1^2),\quad \tau_2=\mu\left(\frac{1}{\lambda_1^2\lambda_2^2}-\lambda_1^2\right),\quad \sigma_m=\mu\left(\lambda_1^2+\lambda_2^2+\frac{1}{\lambda_1^2\lambda_2^2}\right)+\frac{9}{2}\mu\Phi\left(\frac{\lambda_1}{\lambda_2},\lambda_1\lambda_2^2\right), \tag{49}$$

where the parameters $\lambda_1\in(0,+\infty)$ and $\lambda_2\in(0,+\infty)$. By the same token, any stress state lying on the approximate surface $\mathcal{S}_B$ can be written in similar form but with $\Phi=\Psi=1$, namely,

$$\tau_1^B=\mu(\lambda_2^2-\lambda_1^2),\quad \tau_2^B=\mu\left(\frac{1}{\lambda_1^2\lambda_2^2}-\lambda_1^2\right),\quad \sigma_m^B=\mu\left(\lambda_1^2+\lambda_2^2+\frac{1}{\lambda_1^2\lambda_2^2}\right)+\frac{9}{2}\mu, \tag{50}$$

where we have utilized the superscript "B" to avoid notational confusion. Given that the maximum value of Φ is 1 (see Eq. (25)), for any pair of parameters λ_1 and λ_2 we have that $\tau_1=\tau_1^B$, $\tau_2=\tau_2^B$ and $\sigma_m\le\sigma_m^B$, and therefore that the approximate surface $\mathcal{S}_B$ bounds from outside the exact surface $\mathcal{S}$. From the definition of the stress measures (38), it then follows that the approximate surface S_B also bounds from outside the exact surface S in the space of (t_1, t_2, t_3)-stress.

The approximate condition (46) provides then an accurate and mathematically simple cavitation criterion — which can be utilized in lieu of (31) for practical purposes — for Neo-Hookean solids under general loading conditions.

Acknowledgments

Support for this work by the National Science Foundation (USA) through Grant DMS-1009503 is gratefully acknowledged. M.I.I. would also like to acknowledge support from CONICET (Argentina) under Grant PIP 00394/10.

Appendix A. Derivation of the initial-value problem (20)–(21) for $\hat{E}$

This appendix provides the main steps in the derivation of Eqs. (20) and (21), which correspond to the specialization of the initial-value problem (15) to the case of Neo-Hookean materials with stored-energy function (18). We begin by computing the inversion of relations (19)

$$\lambda_1=\Lambda_1^{2/3}\Lambda_2^{1/3}J^{1/3},\quad \lambda_2=\frac{\Lambda_2^{1/3}J^{1/3}}{\Lambda_1^{1/3}},\quad \lambda_3=\frac{J^{1/3}}{\Lambda_1^{1/3}\Lambda_2^{2/3}}, \tag{51}$$

Please cite this article as: Lopez-Pamies, O., et al., Cavitation in elastomeric solids: II—Onset-of-cavitation surfaces for Neo-Hookean materials. J. Mech. Phys. Solids (2011), doi:10.1016/j.jmps.2011.04.016

and recognize, by using the definition $\hat{E}(\Lambda_1,\Lambda_2,J,f_0)\doteq E(\lambda_1,\lambda_2,\lambda_3,f_0)$ and the chain rule, that

$$\frac{\partial E}{\partial\lambda_1}=\frac{\Lambda_1^{1/3}}{\Lambda_2^{1/3}J^{1/3}}\frac{\partial\hat{E}}{\partial\Lambda_1}+\frac{J^{2/3}}{\Lambda_1^{2/3}\Lambda_2^{1/3}}\frac{\partial\hat{E}}{\partial J},$$

$$\frac{\partial E}{\partial\lambda_2}=-\frac{\Lambda_1^{4/3}}{\Lambda_2^{1/3}J^{1/3}}\frac{\partial\hat{E}}{\partial\Lambda_1}+\frac{\Lambda_1^{1/3}\Lambda_2^{2/3}}{J^{1/3}}\frac{\partial\hat{E}}{\partial\Lambda_2}+\frac{\Lambda_1^{1/3}J^{2/3}}{\Lambda_2^{1/3}}\frac{\partial\hat{E}}{\partial J},$$

$$\frac{\partial E}{\partial\lambda_3}=-\frac{\Lambda_1^{1/3}\Lambda_2^{5/3}}{J^{1/3}}\frac{\partial\hat{E}}{\partial\Lambda_2}+\Lambda_1^{1/3}\Lambda_2^{2/3}J^{2/3}\frac{\partial\hat{E}}{\partial J}. \tag{52}$$

With the help of expressions (51) and (52), and in view of the linearity of (18) in the sum of the squares of the principal stretches $\lambda_1^2+\lambda_2^2+\lambda_3^2$, it is then straightforward to compute the corresponding maximizing vector $\boldsymbol{\omega}$ in (15). The solution reads (in component form) as

$$\omega_1=-\frac{\Lambda_1^{2/3}\Lambda_2^{1/3}\xi_1[J(\Lambda_1^2(\Lambda_2^2\xi_3^2+\xi_2^2)+\xi_1^2)-1]}{J^{2/3}[\Lambda_1^2(\Lambda_2^2\xi_3^2+\xi_2^2)+\xi_1^2]}+\frac{\Lambda_1^{7/3}\xi_1(\Lambda_2^2\xi_3^2+2\xi_2^2)}{\Lambda_2^{1/3}J^{1/3}\mu[\Lambda_1^2(\Lambda_2^2\xi_3^2+\xi_2^2)+\xi_1^2]}\frac{\partial\hat{E}}{\partial\Lambda_1}+\frac{\Lambda_1^{4/3}\Lambda_2^{2/3}\xi_1(\Lambda_2^2\xi_3^2-\xi_2^2)}{J^{1/3}\mu[\Lambda_1^2(\Lambda_2^2\xi_3^2+\xi_2^2)+\xi_1^2]}\frac{\partial\hat{E}}{\partial\Lambda_2},$$

$$\omega_2=-\frac{\Lambda_2^{1/3}\xi_2[\Lambda_1^2(J(\Lambda_2^2\xi_3^2+\xi_2^2)-1)+J\xi_1^2]}{\Lambda_1^{1/3}J^{2/3}[\Lambda_1^2(\Lambda_2^2\xi_3^2+\xi_2^2)+\xi_1^2]}-\frac{\Lambda_1^{4/3}\xi_2(\Lambda_1^2\Lambda_2^2\xi_3^2+2\xi_1^2)}{\Lambda_2^{1/3}J^{1/3}\mu[\Lambda_1^2(\Lambda_2^2\xi_3^2+\xi_2^2)+\xi_1^2]}\frac{\partial\hat{E}}{\partial\Lambda_1}+\frac{\Lambda_1^{1/3}\Lambda_2^{2/3}\xi_2[2\Lambda_1^2\Lambda_2^2\xi_3^2+\xi_1^2]}{J^{1/3}\mu[\Lambda_1^2(\Lambda_2^2\xi_3^2+\xi_2^2)+\xi_1^2]}\frac{\partial\hat{E}}{\partial\Lambda_2},$$

$$\omega_3=\frac{1-J}{\Lambda_1^{1/3}\Lambda_2^{2/3}J^{2/3}\xi_3}-\frac{\xi_1\omega_1}{\Lambda_1\Lambda_2\xi_3}-\frac{\xi_2\omega_2}{\Lambda_2\xi_3}. \tag{53}$$

By making direct use of the explicit expressions (53), it is possible to carry out analytically the resulting integrals in (15). In turn, after some algebraic manipulations, the initial-value problem (15) can be finally rewritten as Eqs. (20) and (21) in the main body of the text, where

$$\mathcal{G}_0(\Lambda_1,\Lambda_2,J)=-\frac{3}{2}+\frac{J^{2/3}[(\Lambda_1^2+1)\Lambda_2^2+1]}{3\Lambda_1^{2/3}\Lambda_2^{4/3}}+\frac{\Lambda_1^{1/3}\Lambda_2^{2/3}}{2J^{4/3}}\Gamma_F,$$

$$\mathcal{G}_1(\Lambda_1,\Lambda_2)=\frac{\Lambda_1^3+\Lambda_1}{\Lambda_1^2-1}-\frac{\Lambda_1^2[(\Lambda_1^2+1)\Lambda_2^2-2]}{(\Lambda_1^2-1)(\Lambda_1^2\Lambda_2^2-1)}\Gamma_E+\frac{\Lambda_1^2\Lambda_2^2}{1-\Lambda_1^2\Lambda_2^2}\Gamma_F,$$

$$\mathcal{G}_2(\Lambda_1,\Lambda_2)=-\frac{\Lambda_1^2\Lambda_2}{\Lambda_1^2-1}+\frac{\Lambda_1\Lambda_2[(2\Lambda_1^2-1)\Lambda_2^2-1]}{(\Lambda_1^2-1)(\Lambda_1^2\Lambda_2^2-1)}\Gamma_E+\frac{\Lambda_1\Lambda_2^3}{1-\Lambda_1^2\Lambda_2^2}\Gamma_F,$$

$$\begin{aligned}\mathcal{G}_3(\Lambda_1,\Lambda_2)=&\frac{\Lambda_1^{5/3}\Lambda_2^{1/3}[-(5\Lambda_1^2+3)\Lambda_2^2+2(\Lambda_1^2+1)+(-2\Lambda_1^6+4\Lambda_1^4+\Lambda_1^2+1)\Lambda_2^4]}{3(\Lambda_1^2-1)^2(\Lambda_2^2-1)(\Lambda_1^2\Lambda_2^2-1)}\\&-\frac{\Lambda_1^{8/3}\Lambda_2^{1/3}[(\Lambda_1^2-2)\Lambda_2^2+1][\Lambda_2^2(4\Lambda_1^4\Lambda_2^2-\Lambda_1^2(\Lambda_2^2+7)+\Lambda_2^2-1)+4]}{3(\Lambda_1^2-1)^2(1-\Lambda_2^2)(\Lambda_1^2\Lambda_2^2-1)^2}\Gamma_E\\&+\frac{2\Lambda_1^{8/3}\Lambda_2^{7/3}[-(\Lambda_1^2+1)\Lambda_2^2+(\Lambda_1^4-\Lambda_1^2+1)\Lambda_2^4+1]}{3(\Lambda_1^2-1)(1-\Lambda_2^2)(\Lambda_1^2\Lambda_2^2-1)^2}\Gamma_F,\end{aligned}$$

$$\begin{aligned}\mathcal{G}_4(\Lambda_1,\Lambda_2)=&\frac{\Lambda_1^{8/3}[(\Lambda_1^2+3)(3\Lambda_1^2+1)\Lambda_2^2-4(\Lambda_1^2+1)+(\Lambda_1^6-5\Lambda_1^4-5\Lambda_1^2+1)\Lambda_2^4]}{6(\Lambda_1^2-1)^2\Lambda_2^{2/3}(\Lambda_2^2-1)(\Lambda_1^2\Lambda_2^2-1)}\\&+\frac{\Lambda_1^{11/3}[12\Lambda_1^2\Lambda_2^4-6(\Lambda_1^2+1)\Lambda_2^2+(\Lambda_1^2+1)(\Lambda_1^4-4\Lambda_1^2+1)\Lambda_2^6+4]}{3(\Lambda_1^2-1)^2\Lambda_2^{2/3}(1-\Lambda_2^2)(\Lambda_1^2\Lambda_2^2-1)^2}\Gamma_E\\&-\frac{\Lambda_1^{11/3}\Lambda_2^{4/3}[-(7\Lambda_1^2+1)\Lambda_2^2+(\Lambda_1^4+5\Lambda_1^2-2)\Lambda_2^4+4]}{6(\Lambda_1^2-1)(1-\Lambda_2^2)(\Lambda_1^2\Lambda_2^2-1)^2}\Gamma_F,\end{aligned}$$

$$\begin{aligned}\mathcal{G}_5(\Lambda_1,\Lambda_2)=&\frac{\Lambda_1^{2/3}\Lambda_2^{4/3}(\Lambda_1^2(7-3\Lambda_1^2)\Lambda_2^2-\Lambda_1^2+(4\Lambda_1^6-5\Lambda_1^4-2\Lambda_1^2+1)\Lambda_2^4-1)}{6(\Lambda_1^2-1)^2(\Lambda_2^2-1)(\Lambda_1^2\Lambda_2^2-1)}\\&+\frac{\Lambda_1^{5/3}\Lambda_2^{4/3}((4\Lambda_1^6-6\Lambda_1^4+1)\Lambda_2^6-3(2\Lambda_1^4-4\Lambda_1^2+1)\Lambda_2^4-3\Lambda_2^2+1)}{3(\Lambda_1^2-1)^2(1-\Lambda_2^2)(\Lambda_1^2\Lambda_2^2-1)^2}\Gamma_E\\&-\frac{\Lambda_1^{5/3}\Lambda_2^{10/3}((5-7\Lambda_1^2)\Lambda_2^2+(4\Lambda_1^4-\Lambda_1^2-2)\Lambda_2^4+1)}{6(\Lambda_1^2-1)(1-\Lambda_2^2)(\Lambda_1^2\Lambda_2^2-1)^2}\Gamma_F.\end{aligned} \tag{54}$$

Please cite this article as: Lopez-Pamies, O., et al., Cavitation in elastomeric solids: II—Onset-of-cavitation surfaces for Neo-Hookean materials. J. Mech. Phys. Solids (2011), doi:10.1016/j.jmps.2011.04.016

In the above coefficients,

$$\Gamma_F = \frac{1}{\sqrt{1-\Lambda_2^2}}\mathcal{E}_{\mathcal{F}}\left[\frac{\sqrt{1-\Lambda_2^2}}{2\sqrt{\Lambda_2^2-1}}\ln[2\Lambda_2(\Lambda_2+\sqrt{\Lambda_2^2-1})-1];\frac{\Lambda_1^2\Lambda_2^2-1}{\Lambda_2^2-1}\right],$$

$$\Gamma_E = \frac{1}{\sqrt{1-\Lambda_2^2}}\mathcal{E}_{\mathcal{E}}\left[\frac{\sqrt{1-\Lambda_2^2}}{2\sqrt{\Lambda_2^2-1}}\ln[2\Lambda_2(\Lambda_2+\sqrt{\Lambda_2^2-1})-1];\frac{\Lambda_1^2\Lambda_2^2-1}{\Lambda_2^2-1}\right], \tag{55}$$

where the functions $\mathcal{E}_{\mathcal{F}}$ and $\mathcal{E}_{\mathcal{E}}$ stand for, respectively, the elliptic integrals of first and second kind, as defined by

$$\mathcal{E}_{\mathcal{F}}[\varphi;k] = \int_0^{\varphi}[1-k\sin^2\theta]^{-1/2}\,\mathrm{d}\theta \quad \text{and} \quad \mathcal{E}_{\mathcal{E}}[\varphi;k] = \int_0^{\varphi}[1-k\sin^2\theta]^{1/2}\,\mathrm{d}\theta. \tag{56}$$

Appendix B. Asymptotic solution to (20)–(21) in the limit as $f_0 \to 0+$

In order to solve asymptotically the initial-value problem (20)–(21) for vanishingly small values of f_0, first it is important to recognize that the initial condition (21) is given at $f_0=1$, which corresponds to the opposite end to the neighborhood around $f_0=0$ in the range of physical volume fraction of cavities $f_0 \in [0,1]$. Thus, assuming a certain ansatz for $\hat{E}$ near $f_0=0$ and then expanding the nonlinear pde (20) near $f_0=0$ — as usually done to solve asymptotic problems — is expected to generate a *nested*[10] system of equations for the coefficients introduced in the ansatz. Indeed, this structure is expected to occur because the solution to the initial-value problem (20)–(21) near $f_0=0$ depends, of course, on the initial condition (21) which is given at $f_0=1$, far away from the neighborhood around $f_0=0$. In practice, this means that the computation of the asymptotic solution to (20)–(21) near $f_0=0$ may require, in general, the computation of the full solution to (20)–(21) for all $f_0 \in [0,1]$. Because of the isotropy of the total elastic energy $\hat{E}$ at hand, however, it is possible to construct an asymptotic solution to (20)–(21) near $f_0=0$ without having to compute the entire solution for all f_0, which is obviously a much more involved task. As elaborated in this appendix, the idea is to consider successively the cases of hydrostatic ($\Lambda_1=\Lambda_2=1$), axisymmetric ($\Lambda_2=1$), and general loading conditions, in such a manner that the appropriate initial conditions for the resulting pdes can be written in terms of the deformation variables (Λ_1 and Λ_2) instead of in terms of the initial volume fraction of cavities (f_0).

(I) *Hydrostatic loading conditions*: Thus, we begin by analyzing the special case of hydrostatic loading conditions when

$$\Lambda_1=\Lambda_2=1. \tag{57}$$

For this type of loading, we note that isotropy dictates that

$$\frac{\partial\hat{E}}{\partial\Lambda_1}(1,1,J,f_0) = \frac{\partial\hat{E}}{\partial\Lambda_2}(1,1,J,f_0) = 0, \tag{58}$$

which, after defining $\hat{E}^H(J,f_0) \doteq \hat{E}(1,1,J,f_0)$, allows to simplify the problem (20)–(21) to the form

$$f_0\frac{\partial\hat{E}^H}{\partial f_0} - \hat{E} + (J-1)\frac{\partial\hat{E}^H}{\partial J} + \frac{\mu}{2}\left(2J^{2/3}+\frac{1}{J^{4/3}}-3\right) = 0, \quad \hat{E}^H(J,1) = 0. \tag{59}$$

The initial-value problem (59) admits the following closed-form solution:

$$\hat{E}^H(J,f_0) = \frac{3\mu}{2}\left[\frac{2J-1}{J^{1/3}} - \frac{2J+f_0-2}{(J+f_0-1)^{1/3}}f_0^{1/3} - (1-f_0)\right]. \tag{60}$$

Note that this solution is valid for any $f_0 \in [0,1]$. When $f_0 \to 0+$, (60) reduces asymptotically to

$$\hat{E}^H(J,f_0) = \frac{3\mu}{2}\left[\frac{2J-1}{J^{1/3}}-1\right] - 3\mu(J-1)^{2/3}f_0^{1/3} + O(f_0). \tag{61}$$

(II) *Axisymmetric loading conditions*: Next, we consider the case of axisymmetric loading conditions with

$$\Lambda_2=1. \tag{62}$$

Again, by exploiting isotropy we have the connection

$$\frac{\partial\hat{E}}{\partial\Lambda_2}(\Lambda_1,1,J,f_0) = \frac{\Lambda_1}{2}\frac{\partial\hat{E}}{\partial\Lambda_1}(\Lambda_1,1,J,f_0), \tag{63}$$

[10] That is, the solution for the coefficient of first order depends on the solution for the coefficient of second order, which in turn depends on the solution for the coefficient of third order, and so on so forth.

Please cite this article as: Lopez-Pamies, O., et al., Cavitation in elastomeric solids: II—Onset-of-cavitation surfaces for Neo-Hookean materials. J. Mech. Phys. Solids (2011), doi:10.1016/j.jmps.2011.04.016

which, after defining $\hat{E}^A(\Lambda_1,J,f_0)\doteq\hat{E}(\Lambda_1,1,J,f_0)$, allows to reduce (20)–(21) to the simpler initial-value problem

$$f_0\frac{\partial\hat{E}^A}{\partial f_0}-\hat{E}^A-\frac{3\mu}{2}+\frac{(2+\Lambda_1^2)(1+2J^2)\mu}{6\Lambda_1^{2/3}J^{4/3}}-\frac{3\Lambda_1^{8/3}(2(\Lambda_1^2+2)\sqrt{\Lambda_1^2-1}-3\Lambda_1\ln[2\Lambda_1^2+\Lambda_1\sqrt{\Lambda_1^2-1}-1])}{16\mu(\Lambda_1^2-1)^{5/2}J^{2/3}}$$
$$\times\left(\frac{2\mu(\Lambda_1^2-1)}{3\Lambda_1^{5/3}J^{1/3}}-\frac{\partial\hat{E}^A}{\partial\Lambda_1}\right)^2+(J-1)\frac{\partial\hat{E}^A}{\partial J}=0,\quad \hat{E}^A(\Lambda_1,J,1)=0. \tag{64}$$

As opposed to the problem of hydrostatic loading (59), the problem of axisymmetric loading (64) does not seem to admit a closed-form solution for all $f_0\in[0,1]$. However, a numerical solution can be readily computed. Then, utilizing the full numerical solution as a guide, the behavior of $\hat{E}^A(\Lambda_1,J,f_0)$ in the limit as $f_0\to0+$ can be assumed to be of the asymptotic form

$$\hat{E}^A(\Lambda_1,J,f_0)=\hat{E}_0^A(\Lambda_1,J)+\hat{E}_1^A(\Lambda_1,J)f_0^{1/3}+O(f_0^{2/3}). \tag{65}$$

Substituting this ansatz in the pde $(64)_1$ and expanding around $f_0=0$ leads to a hierarchical system of pdes for $\hat{E}_0^A$, $\hat{E}_1^A$, and higher-order coefficients. The first equation of this system, of order $O(1)$, reads as

$$-\hat{E}_0^A-\frac{3\mu}{2}+\frac{(2+\Lambda_1^2)(1+2J^2)\mu}{6\Lambda_1^{2/3}J^{4/3}}-\frac{3\Lambda_1^{8/3}(2(\Lambda_1^2+2)\sqrt{\Lambda_1^2-1}-3\Lambda_1\ln[2\Lambda_1^2+\Lambda_1\sqrt{\Lambda_1^2-1}-1])}{16\mu(\Lambda_1^2-1)^{5/2}J^{2/3}}$$
$$\times\left(\frac{2\mu(\Lambda_1^2-1)}{3\Lambda_1^{5/3}J^{1/3}}-\frac{\partial\hat{E}_0^A}{\partial\Lambda_1}\right)^2+(J-1)\frac{\partial\hat{E}_0^A}{\partial J}=0. \tag{66}$$

Now, by recognizing that $\hat{E}^A(1,J,f_0)=\hat{E}^H(J,f_0)$, we conclude from (61) that

$$\hat{E}_0^A(1,J)=\frac{3\mu}{2}\left[\frac{2J-1}{J^{1/3}}-1\right], \tag{67}$$

which can be viewed as the initial condition for the pde (66). The solution to the initial-value problem (66)–(67) can then be computed to lead to

$$\hat{E}_0^A(\Lambda_1,J)=\frac{\mu}{2}\left[J^{2/3}\frac{(2+\Lambda_1^2)}{\Lambda_1^{2/3}}-3\right]+\frac{3\mu}{2}\frac{(J-1)}{J^{1/3}}\Phi^A(\Lambda_1), \tag{68}$$

where the function Φ^A is a solution to the ode

$$\Phi^A-\frac{\Lambda_1^2+2}{2\Lambda_1^{2/3}}+\frac{27\Lambda_1^{8/3}}{32(\Lambda_1^2-1)^{5/2}}[2(\Lambda_1^2+2)\sqrt{\Lambda_1^2-1}-3\Lambda_1\ln[2\Lambda_1^2+2\Lambda_1\sqrt{\Lambda_1^2-1}-1]]\left(\frac{4(\Lambda_1^2-1)}{9\Lambda_1^{5/3}}+\frac{\mathrm{d}\Phi^A}{\mathrm{d}\Lambda_1}\right)^2=0, \tag{69}$$

subject to the initial condition

$$\Phi^A(1)=1. \tag{70}$$

Having solved for $\hat{E}_0^A$, the coefficient $\hat{E}_1^A$ can then be determined from the second equation of the hierarchical system, of order $O(f_0^{1/3})$, subject to the initial condition $\hat{E}_1^A(1,J)=-\mu(J-1)^{2/3}$, as dictated by (61). Given that $\hat{E}_1^A$, and the remaining higher-order coefficients in the ansatz (65), are not needed for our purposes, its computation is omitted here.

(III) *General loading conditions*: Finally, we consider the case of general loading conditions. In the limit as $f_0\to0+$, we assume the total elastic energy to be of the asymptotic form

$$\hat{E}(\Lambda_1,\Lambda_2,J,f_0)=\hat{E}_0(\Lambda_1,\Lambda_2,J)+\hat{E}_1(\Lambda_1,\Lambda_2,J)f_0^{1/3}+O(f_0^{2/3}). \tag{71}$$

Substituting this ansatz in the pde (20) and expanding around $f_0=0$ leads to a hierarchical system of pdes for $\hat{E}_0$, $\hat{E}_1$ and higher-order coefficients. The leading order term of these equations, of order $O(1)$, reads as

$$-\hat{E}_0+(J-1)\frac{\partial\hat{E}_0}{\partial J}+\mathcal{G}_0(\Lambda_1,\Lambda_2,J)+\frac{1}{J}\mathcal{G}_1(\Lambda_1,\Lambda_2)\frac{\partial\hat{E}_0}{\partial\Lambda_1}+\frac{1}{J}\mathcal{G}_2(\Lambda_1,\Lambda_2)\frac{\partial\hat{E}_0}{\partial\Lambda_2}$$
$$+\frac{1}{J^{2/3}}\mathcal{G}_3(\Lambda_1,\Lambda_2)\frac{\partial\hat{E}_0}{\partial\Lambda_1}\frac{\partial\hat{E}_0}{\partial\Lambda_2}+\frac{1}{J^{2/3}}\mathcal{G}_4(\Lambda_1,\Lambda_2)\left(\frac{\partial\hat{E}_0}{\partial\Lambda_1}\right)^2+\frac{1}{J^{2/3}}\mathcal{G}_5(\Lambda_1,\Lambda_2)\left(\frac{\partial\hat{E}_0}{\partial\Lambda_2}\right)^2=0, \tag{72}$$

where it is recalled that the coefficients $\mathcal{G}_0$, $\mathcal{G}_1$, $\mathcal{G}_2$, $\mathcal{G}_3$, $\mathcal{G}_4$, $\mathcal{G}_5$ are given explicitly by (54). At this stage, we recognize that $\hat{E}(\Lambda_1,1,J,f_0)=\hat{E}^A(\Lambda_1,J,f_0)$, and hence that

$$\hat{E}_0(\Lambda_1,1,J)=\hat{E}_0^A(\Lambda_1,J), \tag{73}$$

with $\hat{E}_0^A$ denoting the leading order term (68) of the asymptotic axisymmetric solution (65) worked out above. Expression (73) can be considered as the initial condition for the pde (72). The solution to the initial-value problem (72)–(73) can be

Please cite this article as: Lopez-Pamies, O., et al., Cavitation in elastomeric solids: II—Onset-of-cavitation surfaces for Neo-Hookean materials. J. Mech. Phys. Solids (2011), doi:10.1016/j.jmps.2011.04.016

worked out analytically to render

$$\hat{E}_0=\frac{\mu}{2}\left[J^{2/3}\frac{(\Lambda_1^2+1)\Lambda_2^2+1}{\Lambda_1^{2/3}\Lambda_2^{4/3}}-3\right]+\frac{3\mu}{2}\frac{(J-1)}{J^{1/3}}\Phi(\Lambda_1,\Lambda_2), \tag{74}$$

where Φ is the solution to the following first-order nonlinear pde:

$$\begin{aligned}&\mathcal{F}(\Lambda_1,\Lambda_2)\Phi+\mathcal{F}_0(\Lambda_1,\Lambda_2)+\mathcal{F}_1(\Lambda_1,\Lambda_2)\frac{\partial\Phi}{\partial\Lambda_1}+\mathcal{F}_2(\Lambda_1,\Lambda_2)\frac{\partial\Phi}{\partial\Lambda_2}+\mathcal{F}_3(\Lambda_1,\Lambda_2)\frac{\partial\Phi}{\partial\Lambda_1}\frac{\partial\Phi}{\partial\Lambda_2}\\&\quad+\mathcal{F}_4(\Lambda_1,\Lambda_2)\left(\frac{\partial\Phi}{\partial\Lambda_1}\right)^2+\mathcal{F}_5(\Lambda_1,\Lambda_2)\left(\frac{\partial\Phi}{\partial\Lambda_2}\right)^2=0\end{aligned} \tag{75}$$

subject to the initial condition

$$\Phi(\Lambda_1,1)=\Phi^A(\Lambda_1). \tag{76}$$

In the above expressions, the coefficients are given by

$$\mathcal{F}(\Lambda_1,\Lambda_2)=-4(\Lambda_1^2-1)^2\Lambda_2^{2/3}(\Lambda_2^2-1)(\Lambda_1^2\Lambda_2^2-1)^2,$$

$$\mathcal{F}_0(\Lambda_1,\Lambda_2)=4\Lambda_1^{1/3}(\Lambda_1^2-1)^2\Lambda_2^{4/3}(\Lambda_2^2-1)(\Lambda_1^2\Lambda_2^2-1)^2\Gamma_F,$$

$$\mathcal{F}_1(\Lambda_1,\Lambda_2)=12\Lambda_1(\Lambda_1^2-1)\Lambda_2^{2/3}(\Lambda_2^2-1)(\Lambda_1^2\Lambda_2^2-1)\,[-\Lambda_1\Lambda_2^2(-\Lambda_1^2(\Gamma_E+\Gamma_F)-\Gamma_E+\Gamma_F+\Lambda_1^3+\Lambda_1)-2\Gamma_E\Lambda_1+\Lambda_1^2+1],$$

$$\mathcal{F}_2(\Lambda_1,\Lambda_2)=12\Lambda_1(\Lambda_1^2-1)\Lambda_2^{5/3}(\Lambda_2^2-1)(\Lambda_1^2\Lambda_2^2-1)\,[\Lambda_2^2(-2\Gamma_E\Lambda_1^2+\Gamma_E+\Gamma_F(\Lambda_1^2-1)+\Lambda_1^3)+\Gamma_E-\Lambda_1],$$

$$\begin{aligned}\mathcal{F}_3(\Lambda_1,\Lambda_2)=6\Lambda_1^{5/3}\Lambda_2[&\Gamma_E\Lambda_1((\Lambda_1^2-2)\Lambda_2^2+1)(\Lambda_2^2(4\Lambda_1^4\Lambda_2^2-\Lambda_1^2(\Lambda_2^2+7)+\Lambda_2^2-1)+4)\\&+\Lambda_2^2(\Lambda_1(2(-\Gamma_F\Lambda_1^2+\Gamma_F+\Lambda_1^3)+7\Lambda_1)+3)+\Lambda_2^4(2\Gamma_F(\Lambda_1^4-1)\Lambda_1+2\Lambda_1^6-9\Lambda_1^4-1-4\Lambda_1^2)\\&+\Lambda_1\Lambda_2^6(-2\Gamma_F(\Lambda_1^6-2\Lambda_1^4+2\Lambda_1^2-1)-2\Lambda_1^7+4\Lambda_1^5+\Lambda_1^3+\Lambda_1)-2(\Lambda_1^2+1)],\end{aligned}$$

$$\begin{aligned}\mathcal{F}_4(\Lambda_1,\Lambda_2)=3\Lambda_1^{8/3}[&\Lambda_2^2(12\Gamma_E(\Lambda_1^3+\Lambda_1)+4\Gamma_F(\Lambda_1^2-1)\Lambda_1-7(\Lambda_1^2+2)\Lambda_1^2-3)+\Lambda_2^4\\&\times(\Lambda_1(6\Lambda_1^2(\Gamma_F-4\Gamma_E)-7\Gamma_F\Lambda_1^4+\Gamma_F+2\Lambda_1^5+15\Lambda_1^3+8\Lambda_1)-1)+\Lambda_1\Lambda_2^6(-2\Gamma_E\\&\times(\Lambda_1^2+1)(\Lambda_1^4-4\Lambda_1^2+1)+\Gamma_F(\Lambda_1^6+4\Lambda_1^4-7\Lambda_1^2+2)+\Lambda_1^7-5\Lambda_1^5-5\Lambda_1^3+\Lambda_1)+4\Lambda_1(\Lambda_1-2\Gamma_E)+4],\end{aligned}$$

$$\begin{aligned}\mathcal{F}_5(\Lambda_1,\Lambda_2)=3\Lambda_1^{2/3}\Lambda_2^2[&\Lambda_1\Lambda_2^2(6\Gamma_E+\Gamma_F(\Lambda_1^2-1)+2\Lambda_1(\Lambda_1^2-4))+\Lambda_2^4\\&\times(\Lambda_1(6\Gamma_E(2\Lambda_1^4-4\Lambda_1^2+1)+(7\Lambda_1^2-12)\Lambda_1^2(-(\Gamma_F+\Lambda_1))-5\Gamma_F+2\Lambda_1)-1)\\&+\Lambda_1\Lambda_2^6(-2\Gamma_E(4\Lambda_1^6-6\Lambda_1^4+1)-\Gamma_F(\Lambda_1^2-2)+(4\Lambda_1^2-5)\Lambda_1^4(\Gamma_F+\Lambda_1)-2\Lambda_1^3+\Lambda_1)-2\Gamma_E\Lambda_1+\Lambda_1^2+1],\end{aligned} \tag{77}$$

and it is recalled that the function Φ^A is defined by the initial-value problem (69)–(70), and that Γ_F and Γ_E are defined by expressions (55).

While the function Φ, as defined by the initial-value problem (75)–(76), cannot be written in the closed form, it is relatively simple to compute it numerically. In Appendix C below, we spell out the key steps in the numerical computation of Φ and discuss its properties.

Appendix C. The function $\Phi(\Lambda_1\Lambda_2)$

In this appendix, we discuss the numerical computation of the function Φ defined by the initial-value problem (75)–(76), as well as establish its growth conditions and upper and lower bounds.

The numerical computation of Φ requires solving the first-order nonlinear pde (75) subject to the initial condition (76). In this regard, we note that the initial condition (76) itself requires solving numerically the nonlinear ode (69) subject to the initial condition (70). Now, because of its quadratic nonlinearity, it is important to realize that Eq. (76) has two solutions. One of the solutions is always positive, whereas the other solution is unbounded from below and can therefore be negative, as illustrated by Fig. 7. Given that the total energy (74) of the material must be nonnegative, we discard the unbounded solution (i.e., the dotted-line curve in Fig. 7) as non-physical, and utilize the positive solution (i.e., the solid-line curve in Fig. 7) as the initial condition in (76). In a parallel note, we remark that similar care should be exercised in selecting the appropriate solution when dealing with materials other than Neo-Hookean.

Having identified which is the function Φ^A that must be utilized in (76), we are now in a position to compute numerically the solution for Φ. As a result of our choice of Φ^A, in spite of its quadratic nonlinearity, the pde (75) subject to (76) has only one solution for Φ. Fig. 1(a) shows a plot for that solution in a large range of deformations Λ_1 and Λ_2. An important observation from this plot is that in the undeformed configuration (i.e., when $\Lambda_1=\Lambda_2=1$) $\Phi=1$, and that beyond the undeformed configuration (i.e., as Λ_1 and Λ_2 deviate from 1), Φ decreases monotonically along any radial path.

Please cite this article as: Lopez-Pamies, O., et al., Cavitation in elastomeric solids: II—Onset-of-cavitation surfaces for Neo-Hookean materials. J. Mech. Phys. Solids (2011), doi:10.1016/j.jmps.2011.04.016

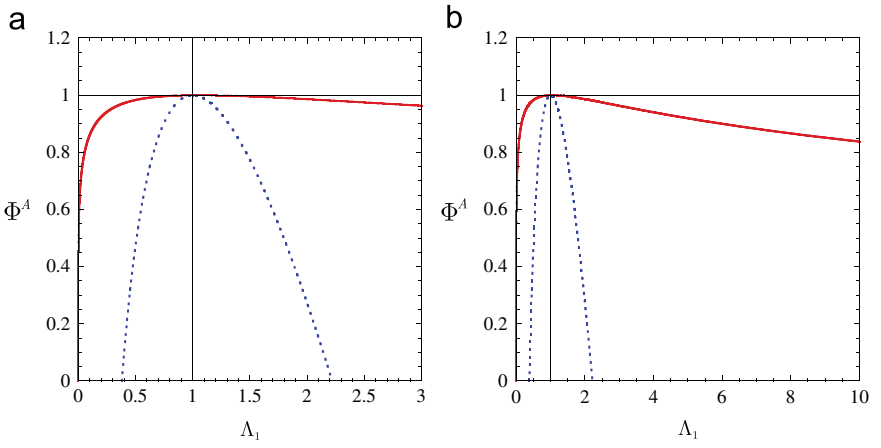

Fig. 7. Plots of the two solutions to the initial-value problem (69)–(70) for Φ^A, as functions of the deformation Λ_1. Part (a) shows a blow up of Φ^A near $\Lambda_1=1$, while part (b) shows results for a larger range of deformations Λ_1. Note that for sufficiently large deformations, as Λ_1 deviates from 1, the dotted-line solution becomes negative. On the other hand, the solid-line solution is always positive. This is the solution that should be used as the initial condition in (76).

The numerical result shown in Fig. 1(a) suggests that $0<\Phi\le 1$ for all $\Lambda_1>0$ and $\Lambda_2>0$. To see that this is indeed the case, we begin by remarking that in the limit of *infinitesimally small deformations* as $\Lambda_1\to 1$ and $\Lambda_2\to 1$, the solution to (75)–(76) can be computed in closed form to render

$$\Phi(\Lambda_1,\Lambda_2)=1-\frac{17-\sqrt{265}}{27}((\Lambda_1-1)^2+(\Lambda_2-1)^2+(\Lambda_1-1)(\Lambda_2-1))+O((\Lambda_1-1)^3)+O((\Lambda_2-1)^3). \tag{78}$$

The solution to (75)–(76) can also be computed in closed form in the limit of *infinitely large deformations*. Indeed, in the limit as $\Lambda_1\to 0$ we have that

$$\Phi(\Lambda_1,\Lambda_2)=\frac{-\Lambda_2^{2/3}}{3\sqrt{1-\Lambda_2^2}}\mathcal{E}_F\left[\frac{\sqrt{1-\Lambda_2^2}}{2\sqrt{\Lambda_2^2-1}}\ln[2\Lambda_2(\Lambda_2+\sqrt{\Lambda_2^2-1})-1];\frac{1}{1-\Lambda_2^2}\right]\Lambda_1^{1/3}\ln\Lambda_1+O(\Lambda_1^{4/3}(\ln\Lambda_1)^2), \tag{79}$$

and from the symmetry $\Phi(\Lambda_1,\Lambda_2)=\Phi(\Lambda_2^{-1},\Lambda_1^{-1})$ due to isotropy we therefore have that in the limit as $\Lambda_2\to+\infty$,

$$\Phi(\Lambda_1,\Lambda_2)=\frac{-\Lambda_1^{-2/3}}{3\sqrt{1-\Lambda_1^{-2}}}\mathcal{E}_F\left[\frac{\sqrt{1-\Lambda_1^{-2}}}{2\sqrt{\Lambda_1^{-2}-1}}\ln[2\Lambda_1^{-1}(\Lambda_1^{-1}+\sqrt{\Lambda_1^{-2}-1})-1];\frac{1}{1-\Lambda_1^{-2}}\right]\Lambda_2^{-1/3}\ln\Lambda_2^{-1}+O(\Lambda_2^{-4/3}(\ln\Lambda_2^{-1})^2). \tag{80}$$

Moreover, in the limit of infinitely large deformation as $\Lambda_1\to+\infty$ the solution to (75)–(76) reduces to

$$\Phi(\Lambda_1,\Lambda_2)=\frac{1}{3\Lambda_2^{2/3}}\Lambda_1^{-2/3}(\ln\Lambda_1^{-1})^2+O(\Lambda_1^{-2/3}\ln\Lambda_1^{-1}), \tag{81}$$

and making again the use of the symmetry $\Phi(\Lambda_1,\Lambda_2)=\Phi(\Lambda_2^{-1},\Lambda_1^{-1})$ we readily deduce from (81) that in the limit as $\Lambda_2\to 0$,

$$\Phi(\Lambda_1,\Lambda_2)=\frac{1}{3\Lambda_1^{-2/3}}\Lambda_2^{2/3}(\ln\Lambda_2)^2+O(\Lambda_2^{2/3}\ln\Lambda_2). \tag{82}$$

At this stage, we recognize from relation (78) that $\Phi(1,1)=1$ corresponds to a local maximum. On the other hand, relations (79)–(82) indicate that $\Phi\to 0$ as the deformation becomes infinitely large, namely, as $\Lambda_1\to 0,+\infty$ and/or $\Lambda_2\to 0,+\infty$. We also recognize that, because the ratio of coefficients $-\mathcal{F}_0/\mathcal{F}\le 1$ for all $\Lambda_1>0$, $\Lambda_2>0$ in the pde (75), the value of Φ evaluated at any critical point (i.e., any point Λ_1, Λ_2 where $\partial\Phi/\partial\Lambda_1=\partial\Phi/\partial\Lambda_2=0$) must be necessarily equal to or less than 1. Then, because $\Phi(1,1)=1$ is a local maximum, $\Phi\to 0$ as $\Lambda_1\to 0,+\infty$ and/or $\Lambda_2\to 0,+\infty$, and there is no local maximum with $\Phi>1$, it follows that

$$0<\Phi(\Lambda_1,\Lambda_2)\le 1\quad\forall\Lambda_1>0,\Lambda_2>0 \tag{83}$$

and that

$$\max_{\Lambda_1,\Lambda_2}\{\Phi(\Lambda_1,\Lambda_2)\}=\Phi(1,1)=1, \tag{84}$$

as pointed out in the main body of the text.

Please cite this article as: Lopez-Pamies, O., et al., Cavitation in elastomeric solids: II—Onset-of-cavitation surfaces for Neo-Hookean materials. J. Mech. Phys. Solids (2011), doi:10.1016/j.jmps.2011.04.016

References

Ball, J.M., 1982. Discontinuous equilibrium solutions and cavitation in nonlinear elasticity. Philosophical Transactions of the Royal Society A 306, 557–611.
Bayraktar, E., Bessri, K., Bathias, C., 2008. Deformation behaviour of elastomeric matrix composites under static loading conditions. Engineering Fracture Mechanics 75, 2695–2706.
Benton, S.H., 1977. The Hamilton–Jacobi Equation: A Global Approach. Mathematics in Science and Engineering, vol. 131. Academic Press.
Chang, Y.-W., Gent, A.N., Padovan, J., 1993. Expansion of a cavity in a rubber block under unequal stresses. International Journal of Fracture 60, 283–291.
Cheng, C., Hiltner, A., Baer, E., 1995. Cooperative cavitation in rubber-toughened polycarbonate. Journal of Materials Science 30, 587–595.
Cho, K., Gent, A.N., Lam, P.S., 1987. Internal fracture in an elastomer containing a rigid inclusion. Journal of Materials Science 22, 2899–2905.
Creton, C., Hooker, J., 2001. Bulk and interfacial contributions to the debonding mechanisms of soft adhesives: extension to large strains. Langmuir 17, 4948–4954.
Fond, C., 2001. Cavitation criterion for rubber materials: a review of void-growth models. Journal of Polymer Science: Part B 39, 2081–2096.
Gent, A.N., 1991. Cavitation in rubber: a cautionary tale. Rubber Chemistry and Technology 63, G49–G53.
Gent, A.N., Lindley, P.B., 1959. Internal rupture of bonded rubber cylinders in tension. Proceedings of the Royal Society of London A 249, 195–205.
Gent, A.N., Tompkins, D.A., 1969. Nucleation and growth of gas bubbles in elastomers. Journal of Applied Physics 40, 2520–2525.
Gent, A.N., Park, B., 1984. Failure processes in elastomers at or near a rigid inclusion. Journal of Materials Science 19, 1947–1956.
Horgan, C.O., Polignone, D.A., 1995. Cavitation in nonlinearly elastic solids: a review. Applied Mechanics Reviews 48, 471–485.
Hou, H.-S., Abeyaratne, R., 1992. Cavitation in elastic and elastic–plastic solids. Journal of the Mechanics and Physics of Solids 40, 571–592.
Lopez-Pamies, O., 2010. A new I_1-based hyperelastic model for rubber elastic materials. Comptes Rendus Mecanique 338, 3–11.
Lopez-Pamies, O., 2009. Onset of cavitation in compressible, isotropic, hyperelastic solids. Journal of Elasticity 94, 115–145.
Lopez-Pamies, O., Idiart, M.I., Nakamura, T. Cavitation in elastomeric solids: I—A defect-growth theory. Journal of the Mechanics and Physics of Solids, in press, doi:10.1016/j.jmps.2011.04.015.
Moraleda, J., Segurado, J., Llorca, J., 2009. Effect of interface fracture on the tensile deformation of fiber-reinforced elastomers. International Journal of Solids and Structures 46, 4287–4297.
Michel, J.C., Lopez-Pamies, O., Ponte Castañeda, P., Triantafyllidis, N., 2010. Microscopic and macroscopic instabilities in finitely strained fiber-reinforced elastomers. Journal of the Mechanics and Physics of Solids 58, 1776–1803.
Nakamura, T., Lopez-Pamies, O. A finite element approach to study cavitation instabilities in nonlinear elastic solids under general loading conditions, submitted for publication.
Polyanin, A.D., Zaitsev, V.F., Moussiaux, A., 2002. Handbook of First Order Partial Differential Equations. Taylor & Francis.
Steenbrink, A.C., Van der Giessen, E., 1999. On cavitation post-cavitation and yield in amorphous polymer-rubber blends. Journal of the Mechanics and Physics of Solids 36, 732–765.
Treloar, L.R.G., 1943. The elasticity of a network of long-chain molecules—II. Transactions of the Faraday Society 39, 241–246.
Treloar, L.R.G., 1944. Stress–strain data for vulcanised rubber under various types of deformation. Transactions of the Faraday Society 40, 59–70.
Xu, X., Henao, D.A. An efficient numerical method for cavitation in nonlinear elasticity. Mathematical Models and Methods in Applied Sciences, in press, doi:10.1142/S0218202511005556.

Please cite this article as: Lopez-Pamies, O., et al., Cavitation in elastomeric solids: II—Onset-of-cavitation surfaces for Neo-Hookean materials. J. Mech. Phys. Solids (2011), doi:10.1016/j.jmps.2011.04.016